2,2-Dithiobis(benzothiazole) complexes (Cd and Ni): Precursors to nanoparticles and electrochemical properties and interactions with Rhodamine B

VUT

Vaal University of Technology

DISSERTATION SUBMITTED IN FULFILMENT OF THE REQUIREMENT FOR THE DEGREE MAGISTER TECHNOLOGIAE: CHEMISTRY IN THE DEPARTMENT OF CHEMISTRY

FACULTY OF APPLIED AND COMPUTER SCIENCES

VAAL UNIVERSITY OF TECHNOLOGY

BY

BUSISIWE DAGRACIA MABASO

SUPERVISOR : PROF M.J MOLOTO (Vaal University of Technology)

CO-SUPERISOR : PROF N. MOLOTO (University of the Witwatersrand)

ACADEMIC YEAR : 2021

DECLARATION

I declare that this work contains no material which has been accepted for the awards of any other degree in any university. To the best of my knowledge, this work contains no material previously published except where the reference has been made in text.

…… …….

Candidate's Signature Date

DEDICATION

This work is dedicated to my parents (Sibongile Mabaso and Albert Mazuze) and my siblings (Fidel, Fiona, Bongani and Fezile).

ACKNOWLEDGEMENTS

I am immensely grateful to God for the good health, courage and strength that was necessary to complete this research project. I wish to express my sincere gratitude to my supervisors Prof M.J and Prof N Moloto for their valuable advice, guidance and support throughout the research project.

This dissertation would be incomplete without the support of my family my parents mother Ms Sibongile Mabaso and father Mr. Albert Mazuze, brothers Fidel, Bongani & Fezile and my sister Fiona I cannot express how important you are in my life.

A special thanks goes to my friends Phindile Mthombo, Lebogang Mogole and Lethabo Mooketsi for keeping me motivated throughout this journey even when I was ready to quit they wouldn't let me. To Modula Damane and Jessica Dlamini thank you for believing in me when I couldn't believe in myself I am truly blessed to call you my friends.

A special thanks goes to Mr. Zondi Nate for taking his time out of his busy schedule and dedicate it on helping me with my work and Mr. Khumbulani Mnqiwu your contributions helped me to finish this work. To Dr Sanni Saheed and Mr. Theo Moundzounga thank you for providing chemicals and assisting me with electrochemistry this work would be incomplete without your help.

I would like to send my gratitude to the NCAP and Nanotechnology group: Dr E.L Viljoen, Dr W Maboya, Dr T Xaba, Dr W Omwoyo, Dr M.G Peleyeju, Prof V Pakade, Prof F.M Mtunzi, Ms D.S More for their guidance, educative and constructive comments and inputs and my fellow postgraduate students W Bout, N Mgedle, O Sentse, M Malatji, Z Nqaba, M Qhubu, C Dikio and A Jawore for creating a friendly working environment. I would forever be indebted to the staff and colleagues in the Department of Chemistry for their suggestions and technical assistance special thanks goes to Dr S.B Sibokoza and P Ngoy for the extra effort.

A special mention must be made to the following people Augustine, Thandolwenkosi, Nsikayethu, Cebolenkosi, Sisekelo, Mvelo, Siphosethu, Zanokuhle, Siyamthanda, Nkosingiphile, Nozipho, Nomfundo, Ziyanda, Busisiwe, Manqoba , Patronella, Langalihle, Welcome and Zinhle I love you all so much thank you for always rooting for my success this dissertation is dedicated to you. Lastly I would like to thank the national research foundation (NRF) and the VUT research directorate for their financial support.

DISSERTATION OUTLINE

This dissertation is divided into 4 chapters. The outline of the chapters is as follows.

Chapter 1:

Introduction, background and Literature review (Literature reports on methods of synthesis, applications) the aim, objectives and problem statement/purpose of the study.

Chapter 2

Research methodology experimental and analytical procedure used for the synthesis of complexes and their nanoparticles as well as review of different characterization techniques.

Chapter 3:

Results and discussion (inclusive of the results and discussion focused on different component of the research objectives and interpretation of the findings)

Chapter 4:

Conclusions and recommendations

References

LIST OF ABBREVIATIONS

DTBTA	2,2-dithiobisbenzothiazole
NP's	Nanoparticles
QD	Quantum dots
SPR	Surface plasmon resonance
HDA	Hexadecylamine
TOPO	Tri-octylphosphine-n-oxide
TOP	Tri-octylphosphine
OLA	Oleylamine
QDs	Quantum dots
NCs	Nanocrystals
1D	1 Dimensions
2D	2 Dimensions
T	Temperature
TGA	Thermal Gravimetric Analysis
PL	Photoluminescence
UV-vis	Ultraviolet visible spectroscopy
FTIR	Fourier transform infrared spectroscopy
NMR	Nuclear magnetic resonance spectroscopy
TEM	Transmission electron microscopy
XRD	X-ray diffraction

RhB	Rhodamine B
DPV	Differential pulse voltammetry
EIS	Electrochemical Impedance Spectroscopy
CV	Cyclic voltammetry
SWV	Square-wave voltammetry
SWCNTs	Single-walled carbon nanotubes
MWCNTs	Multi-walled carbon nanotubes
BDDE	Boron-doped diamond electrode
GCE	Glassy carbon electrode
PCE	Pencil graphite electrode
PANI	Polyaniline

PRESENTATIONS

- Oral presentations :3rd VUT Interdisciplinary Research and postgraduate Conference program 17 &18 2018 :

ABSTRACT

The ligand 2, 2-dithiobisbenzothiazole and it metal complexes have been a subject of interest in various fields but they have found to exhibit remarkable and prevalent biological and pharmacological activities. The ligand tends to coordinate to complexes through the sulfur atom and hence the metal-sulphide bond are good precursor to generate metal sulfide nanoparticles using single-source precursor route. The complexes are generally prepared by reflux for 1 to 2 hours depending on the solvent used to produce very stable solid products and some form in crystalline form. All the prepared nickel and cadmium complexes were characterized using techniques such as elemental analyzer, IR, ^{13}C NMR spectroscopy and thermogravimatric analysis. The data obtained from the spectroscopic analysis was consistent of the coordination of the ligand with the metal ions through the sulphur atoms of the 2,2-dithiobisbenzothiazole moiety. The thermal analysis of the prepared complexes gave a final residue of metal sulphide for both metal complexes. Characterization techniques showed the formation of bidentate complexes for both nickel complex and cadmium complex.

The prepared complexes were then used to synthesize metal sulphide nanoparticles .The nanoparticles were prepared by thermal decomposition method of the single source precursor in a solution of oleylamine (OLA). Two different parameters were investigated temperature and time to study their effect on the size and shape of the nanoparticles. The synthesized nanoparticles were characterized using techniques such as UV-Vis spectroscopy, photoluminescence spectroscopy, and X-ray diffraction analysis and transmission electron microscopy. The temperatures of the reaction have a significant effect on the rate of the reaction that will affect the size and shape of the nanoparticles. This effect was confirmed by the optical properties of the synthesized nanoparticles prepared at different reaction temperatures. The spectra shows that absorption maximum and band edge shift to lower wavelength as the temperature of reaction was progressively increased. This trend is associated to the decrease in particles size of the prepared nanoparticles. TEM images further confirmed that the particles size of the prepared nanoparticles was progressively decreased as the temperature was increased. The time of the reaction is one of the most significant factors in the synthesis of the nanoparticles. The investigation of the time of the reaction yield results that depicted that with increase in time of the reaction, the band edge increases, but relatively at short wavelength to the bulk. Hence, the band edges of the nanoparticles

were blue shifted significantly to the bulk. The results show that with an increase in the time of the reaction, the nanoparticles increases in their size due to Ostwald ripening.

The optimum complexes and optimum nanoparticles were used to further study their electrochemical properties using cyclic voltammetry and electrochemical impedance spectroscopy (EIS) graphs were fitted using the randles circuit and they confirm that the NiS nanoparticles GCE greatly increase the electron transfer rate, probably due to the nanostructured surface property of the NiS nanoparticles. Differential pulse voltammetry (DPV) was used to study the electrochemical behavior and the DPV showed that the current response of Rhb was higher for the optimum temperature NiS nanoparticles compared to all the materials used. There was an increase in the Rhb current response with an increase in pH and pH 7 was used as the optimum pH when Ni- complex was used as a modifier and pH 8 was used as optimum when NiS nanoparticles were used as a modifier. Effect of concentration showed that the NiS nanoparticles for the optimum temperature had a wide linear range and a low detection limit. The method has good accuracy, acceptable precision, and reproducibility. This method provides a novel electrochemical method for determination of RhB.

Table of Content

LIST OF FIGURES

LIST OF TABLES

LIST OF SCHEMES

CHAPTER 1

1. INTRODUCTION

1.1 Background

The chemistry of 2,2-dithiobisbenzothiazole has been drawing a lot of interest due to their extensive applications that range over a variety of scientific subjects such as medicine(Kurzajewska et al., 2018), organic synthesis (Habila et al., 2016)and biochemistry (Marconato et al., 1997)(Dondoni & Merino, 1996). 2, 2-dithiobisbenzothiazole (DTBT) shown in **Fig 1.1** possess rich coordination chemistry since they have four sulphur atoms and two nitrogen atoms which can be used for the coordination to the metal center (Rubino et al., 2017). The sulphur atoms on the DTBTA ligand have an extraordinary impact on these material which allow to stabilise the ions in various oxidation states (Ammar et al., 2018). They exhibit a very rich coordination chemistry with a large variety of transition metals and they have shown different kind of pharmacological properties (Rubino et al., 2018).

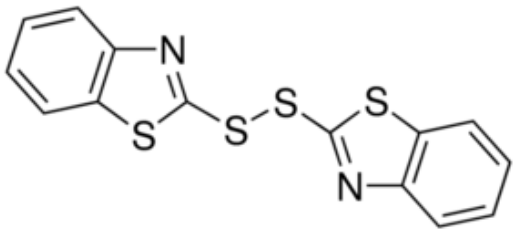

Figure 0.1: Chemical structure of 2,2-dithiobis (benzothiazole) ligand

The bonding of the ligand with the metal center affects the structural architecture, properties and applications of the metal DTBTA complex (Stenger-smith et al., 2018). The current study focuses on the use of the coordination complexes as single source precursor for the synthesis of cadmium sulphide and nickel sulphide nanoparticles (Daravath et al., 2017). Semiconductor nanoparticles are of great scientific interest because of their novel shape and size dependent chemical (Shombe et al., 2016) and physical properties (Mandal et al., 2009) that differ drastically from their bulk counterparts (Bobinihi et al., 2021). In particular metal sulphide materials usually show novel electronic (Suresh, 2013), optical (Riyaz et al., 2016), and magnetic properties (Kumar et al., 2020) due to their quantum size effect and large surface area. Owing to their excellent properties, these

materials exhibit a wide variety of potential applications in nanodevices such as nonlinear optical devices, photocatalytic material and electrochemical sensors. Over the years coordination compounds/complexes have been utilized as single-source precursors for the preparation of nanoparticles (Yang et al., 2019). Several methods have been employed for the synthesis of well dispersed metal sulphide nanoparticles including the sol-gel (Let et al., 2007), colloidal (Kuznetsova et al., 2019) and thermal decomposition methods (Reyes et al., 2014). However thermal decomposition techniques has received much attention compared to other methods because this method allows the control of phase, size distribution, shape and crystalinity of the final product by changing the parameters such as temperature, reaction time capping agent and the precursor (Onwudiwe et al., 2015). Nickel sulphide and cadmium sulphide nanoparticles have been used in different technological applications. Recently they have gained massive interest as electrochemical sensors for the determination of organic dyes due to their high catalytic properties, low cost and good stability.

For several years the misuse of organic dyes has been posing great threats to the environment and human beings (Pathan et al., 2018). RhB dye has been found to be carcinogenic and has been forbidden for use as food additives is some countries (He et al., 2019). However due to it low cost, high stability and high effectiveness, this harmful dye is still illegally used in some part of the world, thus prompting research to develop a simple, fast and sensitive method for the determination of RhB (Pathan et al., 2018). Traditional methods such as spectrophotometry (Baddouh et al., 2018), chromatography (He et al., 2019) and fluorimetric methods (Sengan & Veerappan, 2019) have been used for the detection of RhB, nonetheless these techniques have been found to have drawbacks which hinder their applications. In contrast electroanalytical methods are selective, highly sensitive, inexpensive, less –time consuming with a wide dynamic range and quick response due to the above merits (Kleijn et al., 2014) and electrochemical methods can be considered a suitable method for the determination of RhB. Modification of electrodes to attain high sensitivity, selectivity and compatibility necessitates extensive study. The excellent performance of modified electrodes depends upon various modifiers (Gill et al., 2020) such as carbon materials, conducting polymers and nanomaterials metal. Current research for emerging new electrode material is now focused on the use of semiconductor nanoparticles. Nanomaterial-

modified electrodes have been used for electrochemical studies due to their unusual catalytic and electronic properties that are that are different from their bulk (He et al., 2019).

1.2. Literature review

1.2.1 Coordinating complexes

The coordination chemistry of any transition metal seems to be a complicated function that involves numerous variables. Understanding and predicting the results of the reactions involving transition metal is an ultimate goal in inorganic chemistry (Nyamen et al., 2013). Metal coordination complexes have a wide variety of technological and industrial applications ranging from catalysis (Daravath et al., 2017) to anti-cancer drugs (Shirmohammadzadeh, 2017). In these compounds the metal atom itself may have a number of roles based on it coordination geometry, oxidation state and magnetic electronic and photochemical behavior (Yousif et al., 2017). Benzothiazole and it derivatives are an important class of ligands in coordination chemistry (Stenger-smith et al., 2018) their complexing ability containing different donor atoms are widely reported they are known to form strong chelating complexes with a wide range of metals (Daravath et al., 2017). Coordination compounds containing sulphur atoms as donors have received great attention because of their metal sulphur bonds as well as air and moist stability (Rubino et al., 2017). Recently these properties have been exploited to prepare semiconductor nanomaterials materials using 2,2-dithiobisbenzothiazole complexes as single source precursors (Mensah et al., 2021).

1.2.2. Semiconductor nanoparticles/ quantum dots

Among nanocrystalline semiconductor, metal sulphides are significant due to their optical, electronic and magnetic properties (Cruz Terrazas et al., 2015). Metal sulphide nanoparticles such as CdS and NiS have found applications in sensors, fluorescent biological labelling and electrochemistry (Kuznetsova et al., 2019). The interesting properties of semiconductor nanoparticle are due to electronic quantum confinement effect and large number of exposed atoms on the surface (Suresh, 2013).

1.2.2.1. Cadmium sulphide nanoparticles

Among the various nanoparticles a great interest has been shown towards cadmium sulphide (CdS) nanoparticles (Kumar et al., 2020) because of availability of descrete energy levels (Nyamen et

al., 2013), size dependent optical properties (Ethiraj Sathiyaraj et al., 2017), tunable bandgap (Cruz Terrazas et al., 2015) and a well-developed synthentic protocol (A. S. Pawar et al., 2016), easy preparation technique with good chemical stabiity (Kuznetsova et al., 2019). CdS nanoparticles categorised under the group chalcogenides and are an II –V group semicondoctor nanoparticles with direct band gap of 2.42 eV which shows size depent optical and electrical properties due high surface area to volume ratio and quantum confinement (Moloto et al., 2009). Due to high photosensitivity it has usage in detection of visible radiations , in light emitting diodes, solar cells , photochemicalcatalysis (Yang et al., 2019), gas sensors (Qi et al., 2001) optoelecrronic devices (Antolini et al., 2012) and range of biological applications (M. J. Pawar et al., 2019). Semoconducting optoelectronic materials play an important role in a variety of applications due to their optical , electrical, magnetic and piezoelectric properties (Kucur et al., 2003) .Modification of these properties of semiconductor materials depend upon the size (Kurian et al., 2007) ,morphology (Mandal et al., 2009) and dimension of nanomaterials (Shombe et al., 2016).Due to the size depend of semicondoctors researcherss interest turn towards the synthesis of nanometer range dimension which is comparable to the Bohr radius (Kumar et al., 2020). There are various physical, chemical and biological methods for synthesizing CdS nanoparicles. One of the principal routes to high quality CdS nanoparticles is the thermolysis of metal complexes as single source precursors in high boiling solvensts (Roy et al., 2015).This routes allows the control of particle size and shape by varying reaction conditions such as temperature , precursor concentration and capping group (Onwudiwe et al., 2015).

1.2.2.2 Nickel sulphide nanoparticles

Nickel sulphide nanoparticles are an important family members of transition metal sulphides, it has different stochiometries which makes it more attractive and interesting but complicated to study (Hu et al., 2021). Nickel sulphide system is highly interesting because of the number of its phases including α-NiS, β-NiS, NiS_2, Ni_3S_2, Ni_3S_4, Ni_7S_6, Ni_9S_8 (Shombe et al., 2020) which find use in energy applications (E. Sathiyaraj et al., 2019) .Ni_3S_2 has potential as a low cost counter electrode materials in dye- sensitized solar cells (Kristl et al., 2017), while α-NiS has been used as a cathode material in lithium ion batteries, memory devices and as a photocatalyst (Hu et al., 2021). Nickel sulphide is a p-type semiconductor material with narrow band gap of 0.4 eV (Thangwane et al., 2017).

1.2.3 Methods of nanoparticles synthesis

Several routes have been employed for the synthesis of well dispersed nanoparticles (Suresh, 2013). Generally the technique for the synthesis of nanoparticles are categorized either as top-down or bottom up approach. In the top down synthesis approaches a bulk semiconductor is thinned/ reduced to form nanoparticles (Kristl et al., 2017). High energy milling, inert gas evaporation and electron beam lithography are the most commonly used to obtain nanomaterial, controlled shapes and sizes with the desired packing geometries are achievable for systematic experiments quantum confinement effect (E. Sathiyaraj et al., 2019). Structural imperfection by sputtering and incorporation of impurities into the nanoparticles are the major drawbacks with this method. In the bottom-up approach nanomaterial are built from molecular structures and these structures assemble themselves chemically by molecular recognition principle. A number of different self-assembly techniques have been employed for the synthesis of nanomaterials, they are subdivided into wet-chemical and vapor phase methods (Salavati-Niasari et al., 2013). Hydro/solvothermal (Onwudiwe et al., 2015), sol-gel (Meshram et al., 2015) and hot solution decomposition/ single source precursor method (Reyes et al., 2014) are generally placed in the category of wet-chemical method, this method is the most preferred and mostly used it is favored due to the ease control of size, shape and manipulation of nanoparticles (Qi et al., 2001). Molecular beam epitaxy, liquid metal ion sources are generally categorized under vapor-phase. Most of the vapor phase methods have drawbacks (produce aggregated nanoparticles) that limit their application (Roffey et al., 2016).

1.2.3.1 Hydro/solvothermal methods

Solvothermal synthesis is a process of transforming reactants in a solution and in a closed system usually a stainless steel autoclave which is heated to a certain temperature and high pressure for a particular time (Celine Rose et al., 2016). The reaction temperature is higher than the boiling point of the solvent in this method(Bobinihi et al., 2021). It is generally called hydrothermal method when water is used during the synthesis (Wasly et al., 2018), the hydrothermal synthesis is usually undertaken at a temperature below the supercritical temperature of water (340°C). The drawback of this method includes the prolonged time of synthesis that ranges from 1h to 30 days and the inability to control the shape of the nanoparticles (Roy et al., 2015).

1.2.3.2 Single source precursor method

Metal complexes have been extensively used as precursors to obtain nanomaterial; they show the relationship between synthetic chemistry and coordination chemistry (Xaba et al., 2017). Recently several researchers use metal complexes as a precursor for the preparation of nanoparticles by different methods (Din & Rehan, 2017). Considerable efforts have been dedicated to controlling the size and shape by different synthetic methods including hydrothermal synthesis, microwave, chemical precipitation, solid-state thermal decomposition methods among the different techniques for the preparation of metal sulphide nanoparticles (Chang et al., 2002; Riyaz et al., 2016). Single source precusour method is the most preferred method because it is cheap and uses nontoxic solvent and it is much easy to control process conditions, particle size and purity of the resulted nanoparticles (Reyes *et al.*, 2014). The use of single source precursor (one pot) method have been proven to be efficient route for the synthesis of high quality nanoparticles (Nqombolo & Ajibade, 2016), it involves the thermolysis of the precursor in a high boiling point coordinating/capping solvents such as olaylamine (OLA) or oleic acid (Jejenija, 2016). In this method the metal-chalcogenide bond is present at a complex stage. This method has advantage over the other methods of synthesis because it avoid the use of volatile, prophoric and toxic by-products. In this method the precursor are air stable and moisture stable. The use of this method reduces the chances of incorporating impurities into the nanoparticles and low deposition routes are possible (Sithole et al., 2018).

1.2.4 Reaction conditions

During the synthesis of nanoparticles, reaction conditions such as temperature and time are varied

1.2.4.1 Effect of temperature

Temperature is one of the major factors that contribute significantly on size, shape, and phase of the nanoparticle synthesis. The temperature of the reaction has an effect on particle size with higher temperature favouring large size. The reaction temperature affects the shape of the nanoparticles due to the competition between kinetic and thermodynamic regime (Bobinihi et al., 2018). Crystallographic phase of the initial seed is one the most critical factors during the nucleation process. Sometimes, the seed have a variety of crystallographic phases, but the stable phase is highly dependent on its environment, most commonly temperature. However, the control of

temperature during the nucleation process can result to a crystalline phase of one compound being more favourable over the other (Kucur et al., 2003).

1.2.4.2 Effect of the reaction time

The time of the reaction is major factor in the preparation of nanoparticles. The time has a significant effect in both size and shape, but less effect on the phase of the nanoparticle. The time has a profound effect on the size with long time favoring large particles size (Celine Rose et al., 2016). The effect of time on the morphology is a bit complex, different morphologies were observed with variation in time of the reaction. The formation of different structure with different reaction times can be explained by Ostwald ripening process. During a reaction, a large number of nuclei are formed in a short time through Ostwald ripening process. As the reaction proceeds, the aggregate continuously grows in size and density. In succession, the particles with small size dissolve and recrystallize because of their higher surface free energy when compared to with that of the larger ones (Bobinihi et al., 2018)(Onwudiwe et al., 2015).

1.2.5 Properties of nanoparticles

The reduction of materials dimensions has pronounced effect on its physical properties which may be significantly different from their bulk counterpart. Some physical properties exhibited by nanomaterials are due to the large number of surface atoms (Yang et al., 2019), large surface energy and spatial confinement. When electromagnetic wave passes through a metal particle, the colour exhibited by metallic nanoparticle is due to the coherent excitation of all free electrons within the conduction band leading to an in-phase oscillation that is known as the surface plasmon resonance (SPR) (Kucur et al., 2003).Thus the colour of metallic nanoparticles may change with respect to size due to surface plasmon resonance This unique optical property may also be due to the quantum confinement effect and band gap which arises primarily due to the confinement of electrons with particles with dimensions smaller than the bulk delocalization length. This effect is more pronounced for semiconductor nanoparticles where the band gap increase with decrease in size (Jejenija, 2016). The band gap of a material is the energy required to create an electron at rest at a distance fair enough apart that their columbic attraction is negligible (Shombe et al., 2016). The catalytic, optical, and electronic properties of nanoparticles have resulted in different applications.

1.2.6 Applications of nanoparticles

The very high dispersity (high surface-to-volume ratio), with both physical and chemical properties of the semiconductor has a major influence on their optical and surface properties. The novel properties of semiconductor nanomaterials have attracted significant attention in research and applications in diverse disciplines such as catalysis, sensors, detectors, solar cells, and biomedicine. Among the unique properties of nanomaterials, the movement of electrons and holes in semiconductor nanomaterials is primarily governed by quantum confinement effect (Agostiano et al., 2000).

Nanoparticles have been suggested recently for applications in electrochemistry where quantum confinement effects may be of advantage (Onwudiwe et al., 2015). When electrons are confined to a small domain such as a nanoparticle the system is called a "quantum dot" or zero-dimensional (0-D) structure (Salavati-Niasari & Sobhani, 2012). Then the electrons are behaving like "particles-in-a-box" and their resulting new energy levels are determined by quantum confinement "effects. These new energy levels give rise to a modification of the optoelectronic properties as compared to the corresponding properties determined by the bulk material electronic structure. As a result, discrete energy levels are needed to describe the electron excitation and transport in quantum dots (Manickathai et al., 2008). Quantum confinement effects lead for example to higher energy level transitions as compared to the bulk material observed as a shorter wavelength optical absorption edge, indicated by a spectral "blue shift". Quantum dots can be used also to produce light emitters of various colors by "band-gap tuning" using particle size effects rather than the current complex techniques of synthesizing compound semiconductors. Another advantage of 0-D semiconductor structures stem from the very long lifetime of electrons in the excited states, which is an important requirement in electrochemical applications. This section focuses on the discussion on the application of semiconductor nanomaterials (used as a catalyst) in electroanalytical chemistry for the detection of Rhodamine B dye.

1.2.7 Rhodamine B

Rhodamine B (RhB) shown in **Fig 2.1** a xanthene dye with positive charge is being extensively exploited in paint (Unsal et al., 2014), textile (Al-Kahtani, 2017), plastics (Marinescu et al., 2018), paper and printing industries (Bhat et al., 2020) because of it well established chemistry, it is also used as a model dye in many important biological application. The extensive use of RhB for

industrial and other applications results in its large scale accumulation in the environment especially in the surface and ground water (Al-Kahtani, 2017). The unique chemical structure of RhB endows it with excellent biological and chemical stability (Zhao & Zhu, 2006), therefore the determination of RhB in wastewater is very important for ensuring the safety of human beings (Unsal et al., 2014).

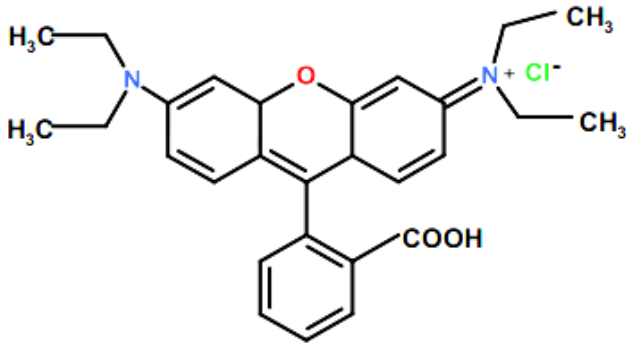

Figure 0.2: Chemical structure of Rhodamine B

1.2.8 Methods for the detection of dyes

1.2.8.1 Traditional methods

Over the years various conventional techniques including high-performance liquid chromatography (HPLC), spectrophotometry, electrophoresis, UV-Vis spectrometry, surface-enhanced Raman spectroscopy, scattering spectroscopy and fluorescence spectroscopy have been used for the determination of RhB (Shah, 2020). Though the detection limits of most these methods are low, complicated sample pretreatment methods which results in time-consuming and not suitable for real-time or field monitoring (Shetti et al., 2019). In addition complex and expensive instruments and skilled operators are necessary for the above methods (Gowthaman et al., 2020).

1.2.8.2 Electroanalytical Methods

Electrochemical analysis has the advantage of rapid response, cheap instruments, simple operation, time-savings, high sensitivity and good selectivity (Bessegato et al., 2019). Electrochemical sensors are suitable tool for rapid and sensitive analysis with wide application (medical, food and environmental) (Baddouh et al., 2018). For two decades modified electrodes have been used as sensors for the electrochemical detection of various electro active molecules like organic dyes.

Electroanalyticatical determination of Rhodamine B is usually performed by pulse voltammetric techniques and sometimes cyclic voltammetry (Shah, 2020):

(i) Cyclic voltammetry

Cyclic voltammetry (CV) is unavoidable in the electrochemical studies however it is surpassed in the field of quantitative measurements (Naja & Bahari, 2016). Cyclic voltammetry remains an indispensable instrument for monitoring the oxidation and reduction mechanism of the analyte as well as a good indicator for possible intermediates. Cyclic voltammograms give five important data cathode and anode peaks corresponding to cathode and anode currents and the value of half potential (Uchida et al., 2018). Those data as well as their mutual relations, are parameters for determining the type of reaction on the electrode (reversible, irreversible or quasi irreversible) (Gomaa et al., 2018). Recently any electrochemical determination of organic or electro active compounds reported they are initiated by running cyclic voltammetry. This is a perfect technique for confirming the success of the modification as well as for finding the optimal conditions, the amount and ratio of the modifiers (Bobinihi et al., 2021). The concrete application of all electrodes modified in various ways is preceded by the precise recording of cyclic voltammogram (Cai et al., 2020).

(ii) Electrochemical impedance spectroscopy (EIS)

Electrochemical Impedance Spectroscopy (EIS) is a very versatile electrochemical tool used to investigate the electrochemical properties of systems and their interfaces with conductive electrodes (Nandhini & Muralidharan, 2018). It is an effective technique for interrogating the kinetics at interfaces and distinguishing between the various mechanisms that govern charge transfer (Tran et al., 2018). EIS can be used in various applications, however in this work it was used to determine the electron transport properties as well as interfacial properties of the modified electrode. The Randles equivalent circuit may be employed to fit the electrochemical impedance data depending on the nature of the impedance data. There are numerous circuits that can be assembled in order to provide the most accurate fit (Khan et al., 2019). An indication of the correct circuit that may be used to fit the data is given by the graphical presentation data is given by the graphical presentation of the impedance data referred to as the Nyquist plot (Li et al., 2013).

(iii) Pulse methods

The key problem of voltammetric measurements is the insufficiently low detection limit as a direct consequence of the occurrence of the capacitive current. The solution to this problem was given by (Barker and Jenkin in 1952) by introducing the pulse methods among electrochemical analysis techniques. The essence of these methods is the same , electrode processes on working electrodes are triggered by pulse potential changes with a constant or increase amplitude, which at the end of the pulse duration results in the measurement of the faradaic current, while at the same time the capacitive current almost completely disappears (Gill et al., 2020). The result of the measurements is the current peak whose height is directly proportional to the concentration of the analyte whose height is directly proportional to the concentration of the analyte. The most commonly applicable are differential pulse voltammetry (DPV) and square-wave voltammetry (SWV). In SWV a potential in the form of symmetric square impulses is applied to the working electrode and the current is recorded at two points one at the end of the pulse, which causes a high value of the oxidative current and one at the end of the pulse responsible for the jump in the reduction current. The resulting voltammogram is bell-shaped and its intensity is proportional to the concentration of the analyte (Chauhan et al., 2020). In DPV the stimulating signal consist of small stepped pulses of constant potential and the current is as in the case of the SWV, recorded in two points.

1.2.9 Electrode material

The effectiveness of electrochemical determinations of Rhodamine B depends on the choice of the appropriate electrode material. An important criteria for choosing a good electrode material is the low background current, wide potential window, reproducibility, stability and electron transfer kinetics. Adsorption is also an important factor because impurities or reaction products can deactivate the electrode, which would require electrode renewal (He et al., n.d.).

1.2.9.1 Carbon paste electrode

Carbon paste electrodes are essentially a mixture of graphite powder and water insoluble organic solvents, which after carefully mixing is packed in a suitable inert container with electrical contact on the side (Marinescu et al., 2018). The greatest advantage of this type of carbon electrode is its surface reproducibility as an important precondition for repeatability of results and low background current. It electrochemical properties depend on the applied organic fluids whose

quantity must be selected so that it is enough to maintain the structure of the electrode, but in limited content, because the transfer of the electron would be disturbed and the background current increased. This electrode is not selective, but considered to be the most suitable for modifications which and has been sometimes used for the detection of different analytes (Alrashdi et al., 2020).

1.2.9.2 Gold and boron-doped diamond electrode

The limitation of application of gold electrode in the cathodic regions results in limitations in the analysis of the reducing substances. This problem is substantially resolved by the application of gold microelectrode and various type of modifiers. While when boron-doped electrode possess some remarkable features when used as a working electrode, compared to conventional carbon and metal electrodes the boron-doped diamond electrode(BDDE) is significantly more inert and chemically stable which makes it suitable for use in extreme chemical conditions such as acidic solutions. In addition it has a wide potential window, high sensitivity and efficiency (Kawde et al., 2016).

1.2.9.3 Glassy carbon electrode

Glassy carbon electrode does not lose it significance, which is not surprising because it has a wide potential widow, it is solid, the surface is renewable and impermeable to gases and it can be applied in negative potential and in the acidic environments (He et al., 2019). It is easily built up and polished and it is functional in the most commonly used solvents. The carbon atoms are sp^2 hybridized and arranged in layers as in the graphite but more densely distributed and impregnation procedures are not required (Tariq et al., 2020). It was found that GCEs are less oxidized in oxygen and carbon dioxide than other carbon materials. Based on literature glassy carbon electrode (GCEs) are used more than the other electrode materials for the determination of Rhodamine B which results in better sensitivity and selectivity (Chauhan et al., 2020).

1.2.10 Different kinds of modifiers.

The excellent performance of modified electrodes depends upon various modifiers such as carbon materials, conducting polymers and metal sulphide nanoparticles

1.2.10.1 Carbon materials

Carbon materials have been extensively used as electrode modifiers and also as electrode materials (Tariq et al., 2020). **Figure 1.3 (A-G)** shows structures of different carbon materials. Carbon

nanotubes (Unsal et al., 2014), grapheme and fullerene are the most utilized carbon materials. Carbon nanotubes exist in the form of single-walled nanotubes (SWNTs) that contains one layer of grapheme curved in the tube Chen et al., 2020) and multi-walled nanotubes (MWNTs) containing several layers in the form of tubes concentrated around the same axis (Unsal et al., 2014) (Nate et al., 2021). They are characterized by good conductivity, stability, flexibility and reactivity. Graphene in it basic form oxide or reduced oxide possess unique physic-chemical properties (Marinescu et al., 2018), very suitable for use among others in electro chemistry (Ali et al., 2018). The behavior of graphene and carbon nanotube is very similar to the behavior of fullerene, the difference lies in the larger surface of graphene due to it one layer structure, in spite of that the chemical activity of graphene is lower than that of fullerene.

He et al., 2019 reported the use of electrochemical application of Cu_2O nanoparticles and electrochemical reduced graphene oxide nano hybrid modified GCE. This modified electrode was then used as a sensor for the catalytic oxidation of Rhodamine B (RhB) and it exhibited an excellent electrochemical performance for RhB. The oxidation potential of RhB was decreased greatly and the sensitivity to detect RhB was improved significantly.

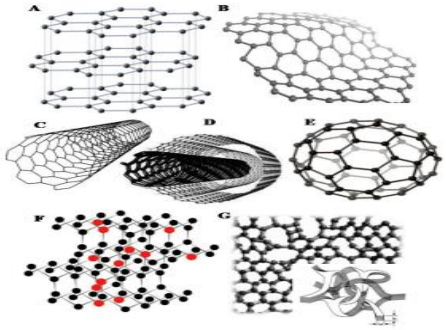

Figure 0.3: Carbon material used as electrode materials and modifiers(A) graphite, (B) grapheme (C) Single-walled carbon nanotubes (D) multi-walled carbon nanotubes, (E) fullerene, (F) boron-doped diamond and (G) glassy carbon

1.2.10.2 Conducting polymers

In year 2000, the discovery of conductive polymers was awarded the Nobel Prize. Since then, significant efforts have been made to develop new conducting polymers and to identify new properties and applications of those materials. Nowadays, conducting polymers are found in a variety of applications and devices, such as organic light-emitting diodes (OLED), antistatic shielding, electrochromism, organic solar cells, supercapacitors, corrosion protection and electrochemical sensors (Bhat et al., 2020). Typical conducting polymers are shown in **Fig. 1.3**. Polyaniline (PANI) is one of the most promising conducting polymers and many studies have been focused on PANI due to its inexpensiveness, easy synthesis, environmental stability, and reversible redox properties (Chen et al., 2020). As an electrochemical sensor material PANI provides abundant electron active sites for binding e.g. toxic chemicals, rapid electron transfer, and tunable conductivity by simple acid-base reactions with different dopants or by incorporating other electro-conductive materials, such as carbon nanotubes, graphene and metal nanoparticles.

Nate et al., reported the use of PANI –cobalt oxide nanoparticles for the determination of antimalarial drugs. They found that the modified electrode showed good reproducibility, selectivity, and sensitivity. Thus, PANI-Co_3O_4 nanocomposite can be used to fabricate electrochemical sensors for quality control purposes. And this study provided a simultaneous electro-oxidation of two different.

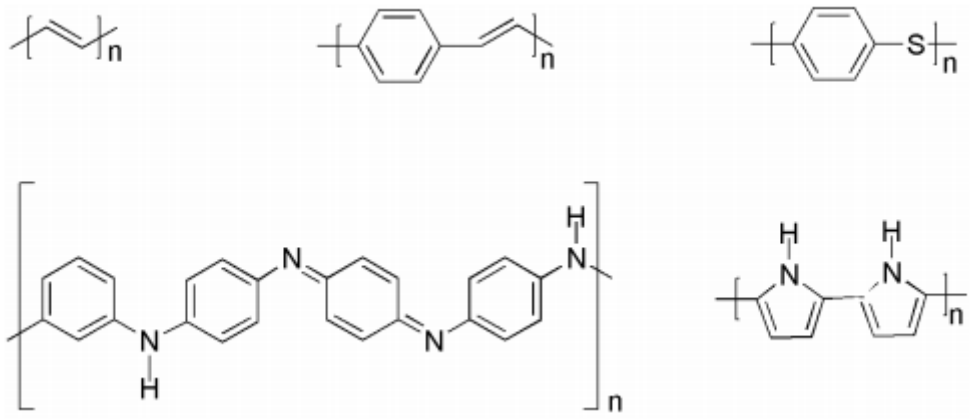

Figure 0.4: Examples of conducting polymers: polyacetylene; polyphenylene vinylene; polyphenyl sulfide; polyaniline; polypyrrole.

1.2.10.3 Nanomaterials.

Intensive effort to improve selectivity and sensitivity in the detection of Rhodamine B has led to a mass introduction of semiconductor nanomaterials in electrochemistry (Pathan et al., 2018). Semiconductor nanoparticles have found tremendous applications in electrochemistry owing to their high surface area, mechanical behavior, and high catalytic performance, and electronic conductivity, low cost and high stability. However these properties are strongly dependent on the synthesis method, the use of single source precursor method for the reparation of nanoparticles suppresses aggregation (Santra et al., 2020) and increase the chance of the nanoparticles to be used as electrochemical sensor (He et al., 2019).

1.3 Overall pointers of the literature review

From the above reviewed literature single source precursor method is the most widely used method for the preparation of nanoparticles because it is inexpensive, easy to set up and also easy to optimize different reaction parameters. Semiconductor nanoparticles have been found to have excellent catalytic and electronic properties and they have a potential of being used as a sensor.

There is little to none existence of literature on the use of nanomaterials without incoorpating them with either carbonic materials or conducting polymers. So in this work, the use of metal sulphide semiconductor nanoparticles were studied as a potential electrochemical sensor and to determine its applicability in this regard.

1.4 Problem statement

According to the International Agency for Research on Cancer (IARC), RhB carries carcinogenic risk: The inhalation, ingestion, and skin contact of RhB may lead to acute and chronic poisoning as well as injury. The illegal use of RhB in different industries has been considered a great threat to human health over the years.

Rhodamine B has been extensively used for fluorescent labelling, cosmetic industry and food coloring due to its fastness, low cost and stability. Moreover, the determination of trace amount of Rhb in water is still a demanding task for ensuring the safety of human beings. At present the analytical methods for the determination of RhB are found to give low detection limit and are complex to operate, however electrochemical methods were found to have fast response, simple

operation and low cost. Up to date there's been a few electrodes developed for the detection of RhB however they have drawbacks which limit their practical applications and make them commercially unfavorable. Therefore, developing a simple modified electrode with high stability, inexpensive and high electrocatayltic activity for RhB detection is still highly demanded for electrochemical analysis.

1.5. Aim

To prepare 2,2-dithiobis(benzothiazole) cadmium and nickel complexes as precursors to nanoparticles and their electrochemical interactions with Rhodamine B.

1.6. Objectives:

- To prepare Cd-DTBTA and Ni-DTBTA complexes using direct synthesis method.
- To characterize the synthesized complexes using elemental analysis, melting point analysis, TGA, FTIR and NMR spectroscopy.
- To prepare CdS and NiS nanoparticles through thermal decomposition of complexes by varying parameters such as temperature (100, 150 and 200 ºC) and time (2hr, 2hr30 min and 3hr).
- To characterize the synthesized nanoparticles using UV-Vis, PL spectroscopy, TEM and XRD
- To evaluate the electrochemical properties of the complexes and the nanoparticles using EIS and CV.
- To evaluate the electrochemical behavior of complexes and nanoparticles towards Rhodamine B dye
- Method development for electrochemical detection of Rhodamine B using the optimum complexes and nanoparticles (studying the effect of pH, concentration and reproducibility)

1.7. Motivation of the electrochemistry in the study

The advancement in nanomaterials are helping to develop electrochemical sensors with increased sensitivity that can be extensively applied to a wide variety of analytical problems including clinical, medicinal, drug delivery, food and environmental areas. Electrochemical methods have proven to be more cost effective, simple, user friendly, portable and faster than other analytical methods. Therefore there is a need to design and develop high-speed and high performance electrochemical sensors that can hold an outstanding ability among analytical devices available for environmental applications. However the success of electrochemical sensing device is determined by the electrode method of synthesis type of electrode as well as modifiers

Therefore this work describe the synthesis of a novel electrochemical sensor and the modification of the sensor derived from cadmium and nickel complexes used as single source precursors to form CdS and NiS nanoparticles modified glassy carbon electrode (GCE), to establish the electrochemical properties of the sensor as well as to determine electrocatayltic ability of the modified electrodes towards the detection of Rhodamine B dye.

CHAPTER 2

2. RESEARCH METHODOLOGY

2.1. Materials and reagents

Nickel (II) chloride hexahydrate ($NiCl_2$•$6H_2O$, 99.9%), Cadmium acetate hydrate [Cd (CH_3CO_2)$_2$], 99.9%), potassium phosphate (KH_2PO_4, 98%), sodium phosphate ($NaPO_4$, 97%), tetrabutylammonium hydroxide (C_4H_9)$_4$NOH, 98%), 2,2-dithiobisbenzothiazole (96.0%), dimethylacetamide [(CH_3CN (CH_3)$_2$, 99.5%], dichloromethane (CH_2Cl_2, 99.8%), aluminium oxide powder (Al_2O_3, 99.9%), potassium ferrocyanide [K_4[Fe(CN)$_6$]•$3H_2O$, 98%], oleylamine ($C_{18}H_{35}NH_2$,70%), oleic acid ($C_{18}H_{34}O_2$, 90%), dimethylsulphoxide (DMSO, 99.5%), dimethylformide (DMF, 99.9%), triethylenetetramine, methanol (CH_3OH, 99.8%), ethanol (C_2H_5OH, 99.8%). All the chemicals were purchased from Sigma Aldrich in South Africa, commercially available AR grade reagents, they were used as received without further purification or modification.

2.2. Preparation of the complexes

2.2.1. Preparation of 2, 2-Dithiobisbenzothiazole Nickel (II) Complex

The nickel chloride hexahydrate was dissolved in methanol and the ligand (2.2-dithiobisbenzothiazole) was dissolved in dichloromethane, the mixture was refluxed for 3 hours at 60℃. The formed green precipitate was filtered washed with excess methanol after cooling, a lime green precipitate was formed and air dried. The lime green product was weighed and characterized. Percentage yield: 74%. Melting point: (200-208 °C). Elemental analysis; found (calcd) % C 49.55(48.02), H 2.49(2.30) N 8.33(8.00) S 38.46(36.62). Significant IR bands (cm^{-1}): LIGAND C=N *v* (1471),C-N v(1009), (C-S) (669)Ni-DBT C=N *v*(1470), C-N (1034), C-S *v*(798) ^{13}C NMR DMSO (d_6) 75 MHz δ(ppm) for the ligand : 148 (C_2) , 126.78 (C_8 C_9) ,128.35 (C_4 C_7), 122.21 (C_5C_6), for complex: 167.32 (C_2), 153.91 (C_2) ,135.67 (C_8), 127.23(C_8), 127.01(C_7), 125.62 (C_4) ,124.29(C_4), 122.49 (C_6), 122.4 (C_5) 40 (DMSO)

2.2.2. Preparation of 2,2-Dithiobisbenzothiazole Cadmium (II) Complex

Cadmium acetate dehydrate was dissolved in methanol and ligand (2,2-dithiobisbenzothiazole) was dissolved dichloromethane and the mixture was refluxed with constant stirring for 3 hours at

0 °C using ice bath. The precipitate formed pale yellowish precipitate was filtered and washed with excess methanol and dried in open air. The pale-yellow product weighed and characterized. Percentage yield: 68%. Melting point: (150-155°C). Elemental analysis; found (calcd.) %; C 46.49(46.4), H 2.48(2.2) N 8.47(7.7), S 36.70(35.4). Significant IR bands (cm^{-1}): LIGAND C=N v(1471), C-N v(1009), 692v(C-S) Cd-DBT C=N *v*(1451), C-N v(1022), C-S v(692), ^{13}C NMR DMSO d_6 75 MHz δ(ppm) for the ligand : 148 (C_2) , 126.78(C_8 C_9) ,128.35 (C_4 C_7), 122.21(C_5C_6), for complex : 151.47 (C_2), 137.29 (C_8), 125.74(C_4) ,124.29(C_4), 122.71 (C_6), 120.98 (C_5), 177.49(C_5), 40 (DMSO).

2.3 Synthesis of the metal (Cd and Ni) sulphide nanoparticles.

The metal sulphide nanoparticles were prepared using the same procedure for both the metal complexes .The nanoparticles were synthesized at various reaction temperature (100, 150 and 200 °C and various reaction times, typically a 0.5 g complex was weighed and dissolved in about 5 mL of oleic acid different reaction times while separately OLA (oleylamine) was heated to 100 °C. After a complete dissolution of the complex the resulting solution was injected into a hot OLA (oleylamine) which was heated and maintained at 100°C with a constant stirring for 1 hour. After an hour the solution was cooled at 70 °C and excess of methanol was added to flocculate the solution. The precipitate formed were isolated by centrifuge washed with methanol three times to remove some of the capping agent and dried in open air environment. For the second part of the environment the reaction was the same as the first part expect that the temperature was maintained at 200°C and the time was varied from (2, 2,5 and 3 hours) the optimum temperature and optimum time were further used for electrochemical processes.

2.4 Electrochemical characterization of complexes and nanoparticles

2.4.1 Preparation of the electrode

The 3 mm in diameter glassy carbon electrode (GCE) was polished with 0.05 µm of alumina slurry and then washed with methanol then dried under infrared lamp. A 5 µL dispersion of Cd-DTBTA/GCE was dried on the surface of the GCE at room temperature. The Cd-DTBTA/GCE was prepared by immersing the Cd-DTBTA/GCE in a phosphate buffer solution (pH 7.0) other modified electrodes were prepared in a similar way.

2.4.2 Electrochemical properties of complexes.

Cyclic voltammetry studies were carried out on AC-LAB potentiostat with a three-electrode cell containing a glassy carbon as the working electrode, Ag/AgCl reference electrode and Pt wire as the counter electrode. Prior to each experiment the glassy carbon electrode was properly cleaned by using Alumina suspension. 0.1 mM solution of the ligand and complexes in DMSO and tetrabutylammonium hydroxide (TBAOH) (0.1 M) as a supporting electrolyte were degassed using nitrogen gas all compounds were investigated in room temperature and voltammograms were recorded at a potential scan rate of 50 $mV.s^{-1}$.

2.4.3 Electrochemical characterization

Electrochemical Impedance Spectroscopy and Cyclic Voltammetry. A 1 mg of the synthesized nanoparticles and complexes were respectively dispersed into 1 mL of the DMF to form a suspension through ultra-sonication before modification of the. The glassy carbon electrode is cleaned by using the method mentioned above. For preparing of the complexes /nanoparticles solution was coated onto the surface of the GCE and allowed to dry under an infrared lamp.

2.5 Experimental details Rhodamine B for sensing

2.5.1. Experimental set up

All electrochemical experiments were carried out at room temperature using a three-electrode system. A modified GCE and a platinum wire served as the working and counter electrodes, respectively and an Ag/AgCl electrode was used as the reference electrode.

2.5.2. Preparation of the working electrode

Before modification, the bare GCE was polished to a mirror-like appearance with a 0.05 then 1μm alumina slurry, then washed successively with anhydrous alcohol and redistilled water in an ultrasonic bath for 1 min, and then dried. The working electrode was prepared as follows: 15μL of modifier dispersion was added onto the prepared GCE surface and dried. The obtained electrode was referred as Cd-DTBTA/GCE. The modification of GCE with other materials followed similar procedure.

2.5.3. DPV experimental procedure for analytes detection

The modified electrode was immersed in 10.0 mL of 0.1M phosphate buffer (pH =7.6), containing Rhb, then the three electrodes were dipped into the electrochemical cell and a potential was applied to the solution from the potentiostat. Finally, the differential pulse voltammograms were recorded,

and the peak currents were read. The parameters for differential pulse voltammetric analysis are as follows: scan rate of 10 mV/s, applied potential from 0 V to 0.8 V, 25 mV of pulse height, 5 mV of step height, 100 ms of pulse width, and 0.5 s of step time.

2.6 Instrumentation

2.6.1 FT-IR Spectroscopy

FIR spectroscopy was used to confirm the functional groups denoting the adsorption of the ligand on the metal surface that results in the formation of the complex. Infrared spectra were recorded on FT-IR Perkin Elmer 400 spectrometer. The spectra were collected over the range from 500-4000 cm^{-1}.

2.6.2 Elemental analysis

Elemental analysis was used to check the percentage composition of C, H, N and S. The elemental analysis is carried out with Leco-CHNS 932 analyzer. Roughly 2.0 mg of the sample was introduced into Ag capsule and was placed in a furnace, which was maintained at 800. The products of combustion in the CHNS analysis (CO_2, H_2O and SO_X gases) were carried through the system by the He carrier. Adjustments for blank, calibration and weights were applied to the final integrated signal and the results were displayed as weight percent of carbon, hydrogen, nitrogen and sulphur.

2.6.3 Thermogravimatric analysis (TGA)

TGA was performed on a PerkinElmer Pyris 6 manager TGA under an inert atmosphere of dry nitrogen and a heating rate of 10°/min using an alumina pan as a reference. The sample preparation for thermogravimatric analysis was done by weighing 10-15 mg of the sample. The samples were decomposed at a temperature ranging from 30 to 900 °C. Thermal analysis was used to determine the temperature at which the material decomposed and the stability of the material.

2.6.4 Solid state nuclear magnetic resonance (NMR) spectroscopy

Solid state NMR experiments were carried out using 4 mm and 2.5 mm outer diameter zirconia (Bruker, Karlsruhe, Germany), ^{13}C NMR spectra were obtained with a Bruker Advance 111 HD MHz (11.1Telsa) standard bore spectrometer and either a double beam resonance BBO 44 or triple channel broad band probe ($Trigamm_{TM}$MAS probe) at a magnetic angle spinning rate of KHz frequency of 125.8 MHz The ^{13}C spectra were reported as ppm. NMR spectroscopy was also used to study the structure of the molecule.

2.6.5 Optical characterization

UV-Vis and PL spectroscopy were used to determine the optical properties of the nanoparticles. Absorption spectra of the particles were measure using a Perkin Elmer Lambda 20 UV-Vis spectrophotometer. The samples were placed in quartz cuvettes (1-cm path length) with toluene as the solvent. Emission spectra of the particles were recorded on a Perkin Elmer LS 45 PL spectrometer with xenon lamp at room temperature. The samples were placed in a glass cuvettes (1cm) with toluene as the solvent.

2.6.6 Transmission Electron Microscopy (TEM)

TEM was used to determine the morphology of the particles. Analysis were done on a LEO JEM 912 electron microscope with an acceleration voltage of 120KW a tungsten wire filament. The samples were prepared by placing a drop of dilute solution of sample in toluene on to a copper grid. The sample was allowed to dry completely at room temperature.

2.6.7 X-ray diffraction analysis

XRD was used to reveal the crystalline nature of the nanoparticles. X-ray diffraction (XRD) patterns on powdered samples were carried out in the 2θ on a D8 diffractometer. Samples were placed in silicon zero background sample holder. Measurements were taken using a glancing angle of incidence detector at an angle of 2°using CuKa1 source, for 2θ values over 20° – 90° in steps of 0.05° with a scan speed of 0.01°2θ.s-1.

2.6.8 Cyclic voltammetry

Electrochemical analyses were conducted on a Bio-Logic SP-240 potentiostat electrochemical workstation. Bare electrode (GCE), Cd complex/GCE and Ni complex/GCE sensors were electrochemically characterized using CV in a solution containing $[Fe(CN)_6]^{3-/4-}$, this was done by cycling a potential from -800 mV to 200 mV at a scan rate of 50 mV/s, to compare the peak current signal of the bare GCE and the modified working electrodes.

2.6.9 Electrochemical Impedance Spectroscopy (EIS)

The parameters for Electrochemical Impedance Spectroscopy (EIS) analysis are: frequency range from 100 kHz to 40 MHz, sinus amplitude of 5 mV and 0.1 of period before each measurement (P_w). The EIS data were analyzed using Z fit software.

CHAPTER 3

3. RESULTS AND DISCUSSIONS

3.1 Complexes

The preparation of metal complexes is the most important step to develop metal complexes which exhibit unique properties and novel reactivity. Nickel and cadmium complexes were formed through the coordination of the metal salt with 2.2-dithiobisbenzothiazole ligand. Sulphur donors bind more strongly to metals than nitrogen hence forming stable complexes when bonded to sulphur. FT-IR, elemental analysis, melting point analysis and NMR spectroscopy have been used to characterize the complexes

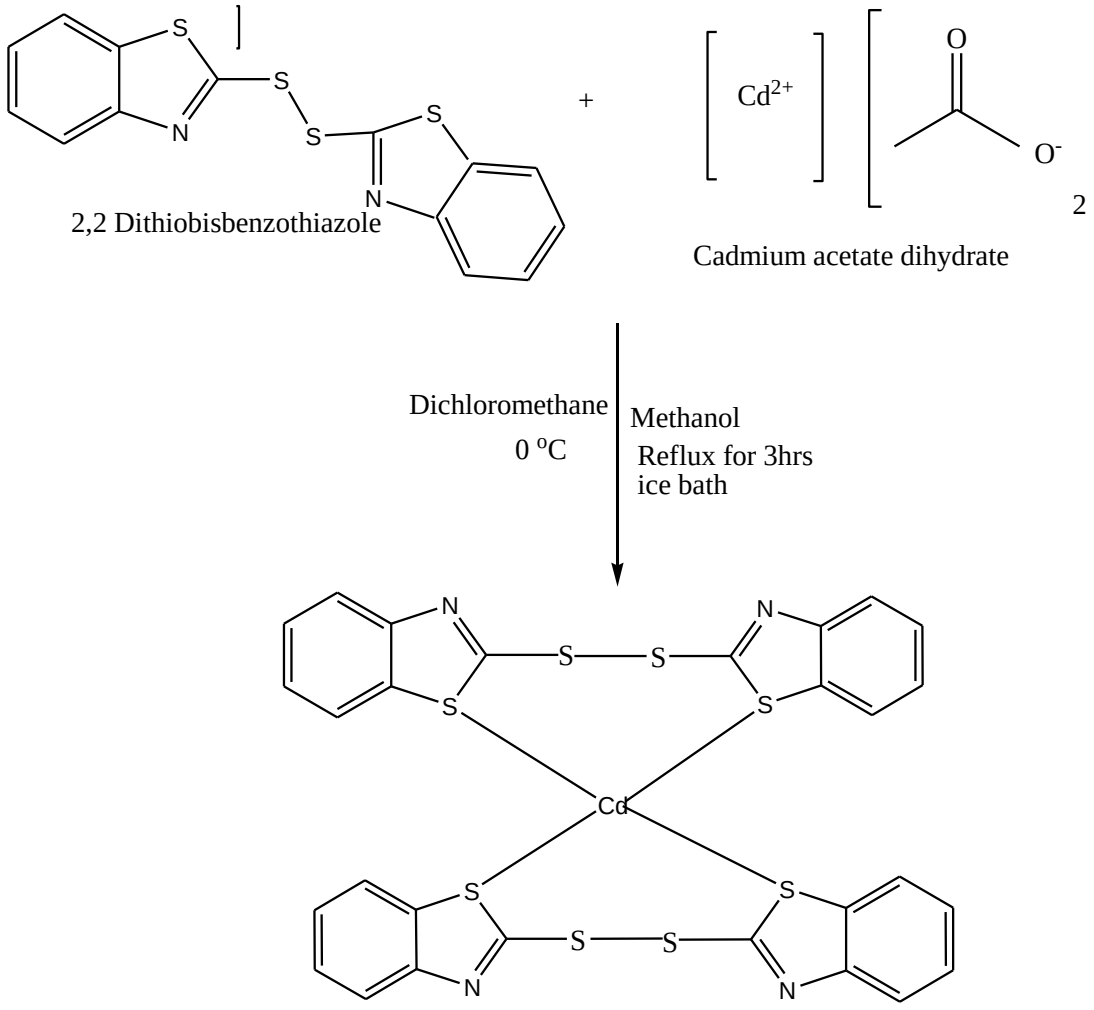

Schemes3.1: Reaction for the formation of Cd-DTBTA complex

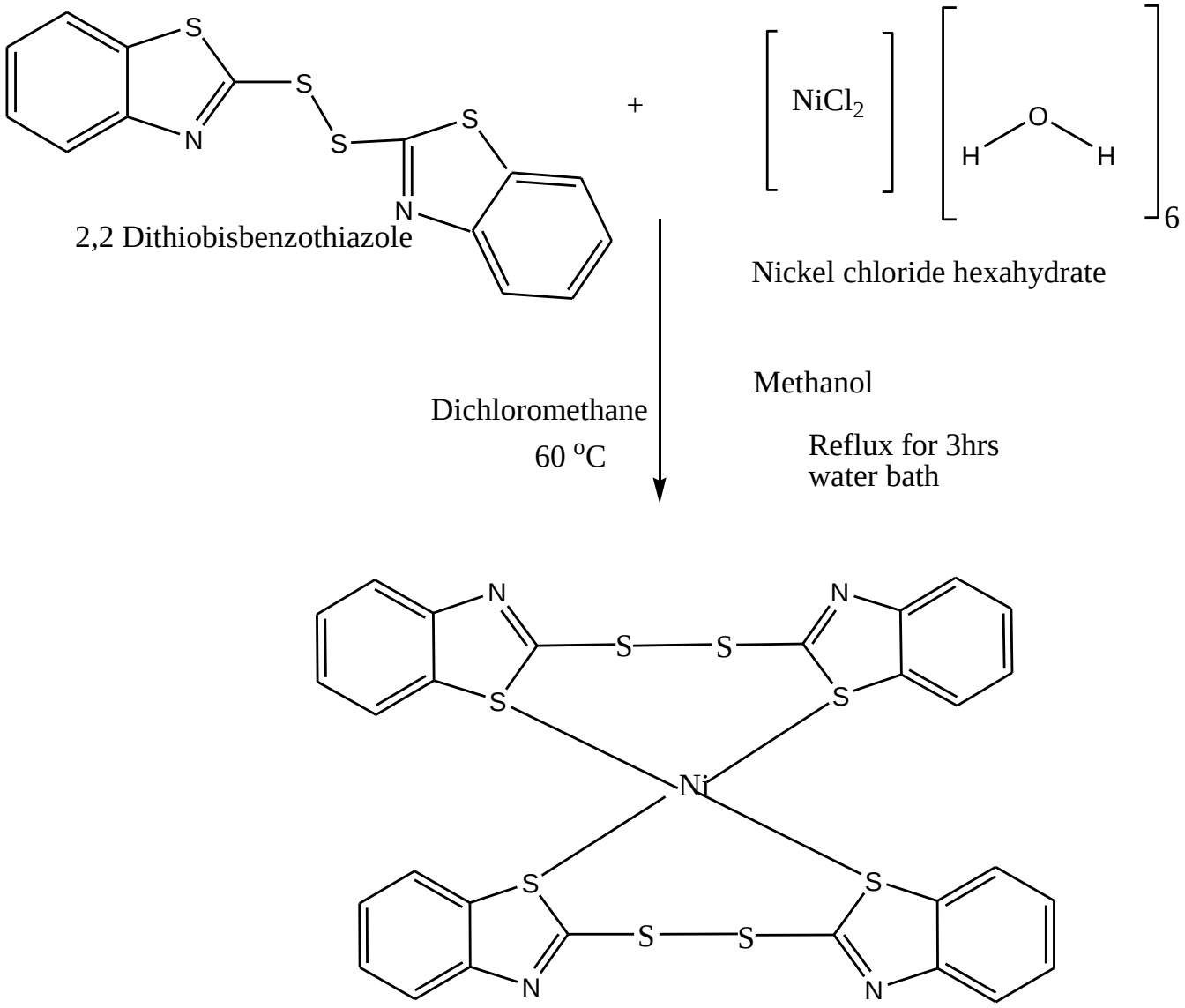

Schemes 3.2: Reaction for the formation of Ni-DTBTA complex.

3. 1.1. Spectroscopic studies

3.1.1FT-IR spectroscopy of Cd-DTBTA and Ni-DTBTA complex

The FT-IR spectroscopy was used to study the functional groups present on the ligand and the formation of new bonds upon complexation. 2,2-dithiobisbenzothiazole ligand has been used over the years and it was found to be capable of forming bonds with metal through the sulphur atom.

2,2-dithiobisbenzothiazole compounds are known to exhibit at region between 500 and 1500. The IR spectra of the ligand shows four characteristic peaks due to stretching vibrations (C=N), (C-N), (C=C) and (C-S) respectively. In the IR spectra of complex (i) and (ii) which are shown in **Fig 3.1** and **3.2** respectively. The characteristic bands due to (C=N) and (C-S) vibrations are shifted after complexation of the ligand to metal ions for both the complexes. This confirms the coordination through sulfur of the ligand. **Table 3.1** shows selected IR values of selected bands of interest of complex (I and II) and the free ligand (III).

The interaction of DTBTA ligand with cadmium acetate to form 2,2-dithiobisbenzothiazole complex was studied using FTIR spectroscopy. **Fig 3.1** shows the IR spectra of the cadmium-DTBTA complex and the ligand. The spectra of the complex is always predicted that there should be a shifting of particular bands to higher or lower frequencies upon complexation due to electron density around the metal atom. In this case there was a shift of v (C=N) to lower frequencies from 1451 cm^{-1} of the ligand to 1470 cm^{-1} for the complex the shift in the complex to lower frequencies is due to the electron donation of the nitrogen atom to the sulphur atom. and there was a splitting of the complex band which was not expected and can be due to impurities of the unreacted ligand .The peak at 1022 is attributed to C-N which is also shifted to higher frequencies in the complex from the ligand of 1009 cm^{-1}. The v C-S appeared at lightly higher frequencies than that of the ligand with a very strong intense single peak without any splitting this phenomena appears to be due to the coordination of the sulphur atom to the metal ion which indicate bidentate binding of the 2,2-dithiobisbenzothiazole to the Cadmium atom as shown in **Scheme 3.1** of the formation of the cadmium complex. This suggest the bonding via the C-S moiety with the metal ion.

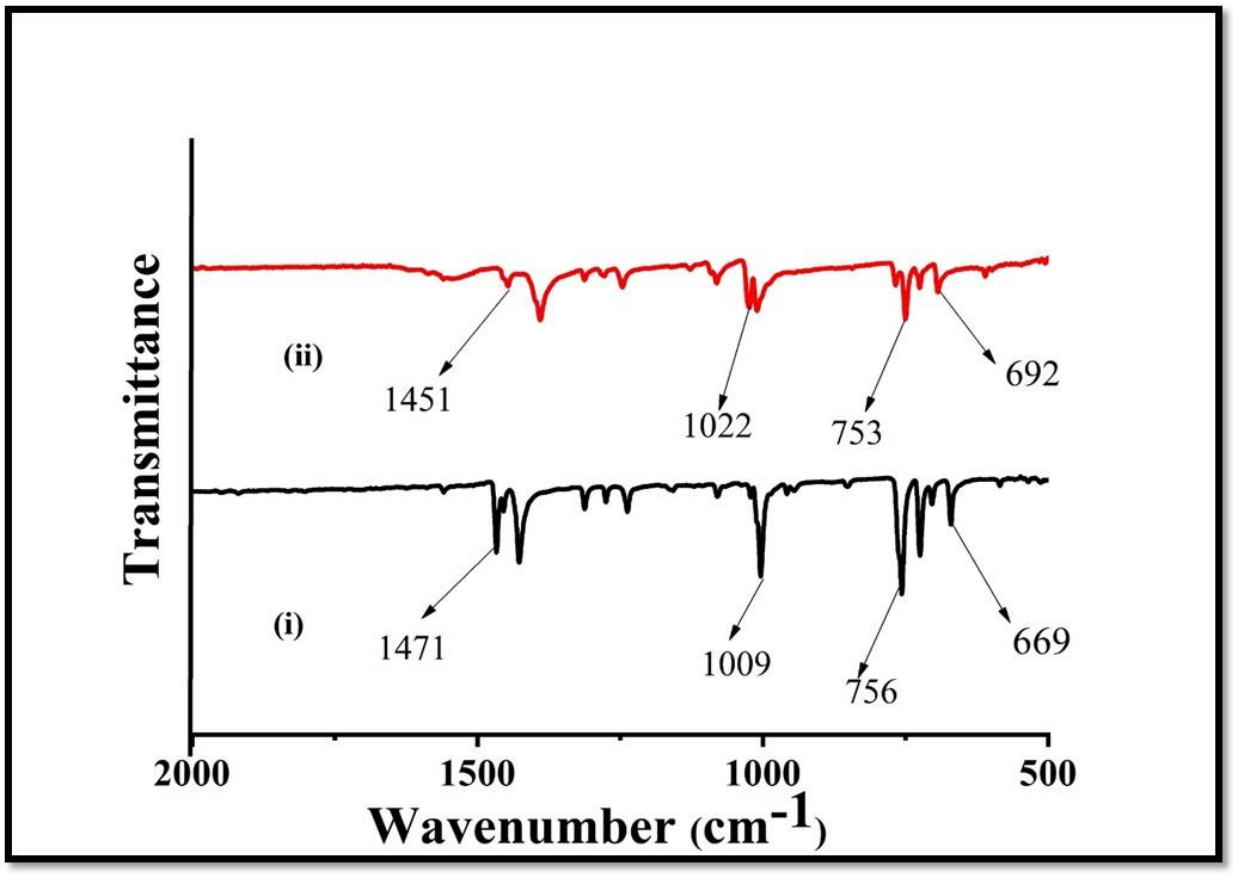

Figure 0.1: FT-IR spectra (i) uncoordinated ligand (ii) Cd-DTBTA complex

Fig 3.2 shows the IR spectra of the [Nickel (DTBTA) $_2$] complex compared with the free DTBTA ligand in order to determine the coordination sites that may be involved in chelating. The (C=N) vibration of the complex was observed with shift from 1471 cm^{-1} of the ligand to 1470 cm^{-1} of the complex. The shift to lower frequencies after complexation was due to electron donation of the nitrogen tom to the sulphur atom. The symmetrical band at 798 cm^{-1} range of the complex is attributed to the contribution of C-S bond, the shift to higher frequencies is due to the increased electron density in the Nickel ion upon complexation. The strong intense single peak without splitting suggest a bidentate bonding with the DTBTA ligand. Similar results have been reported by Goswabi et al., 2015 and Rubino et al., 2017 for the preparation of metal complexes.

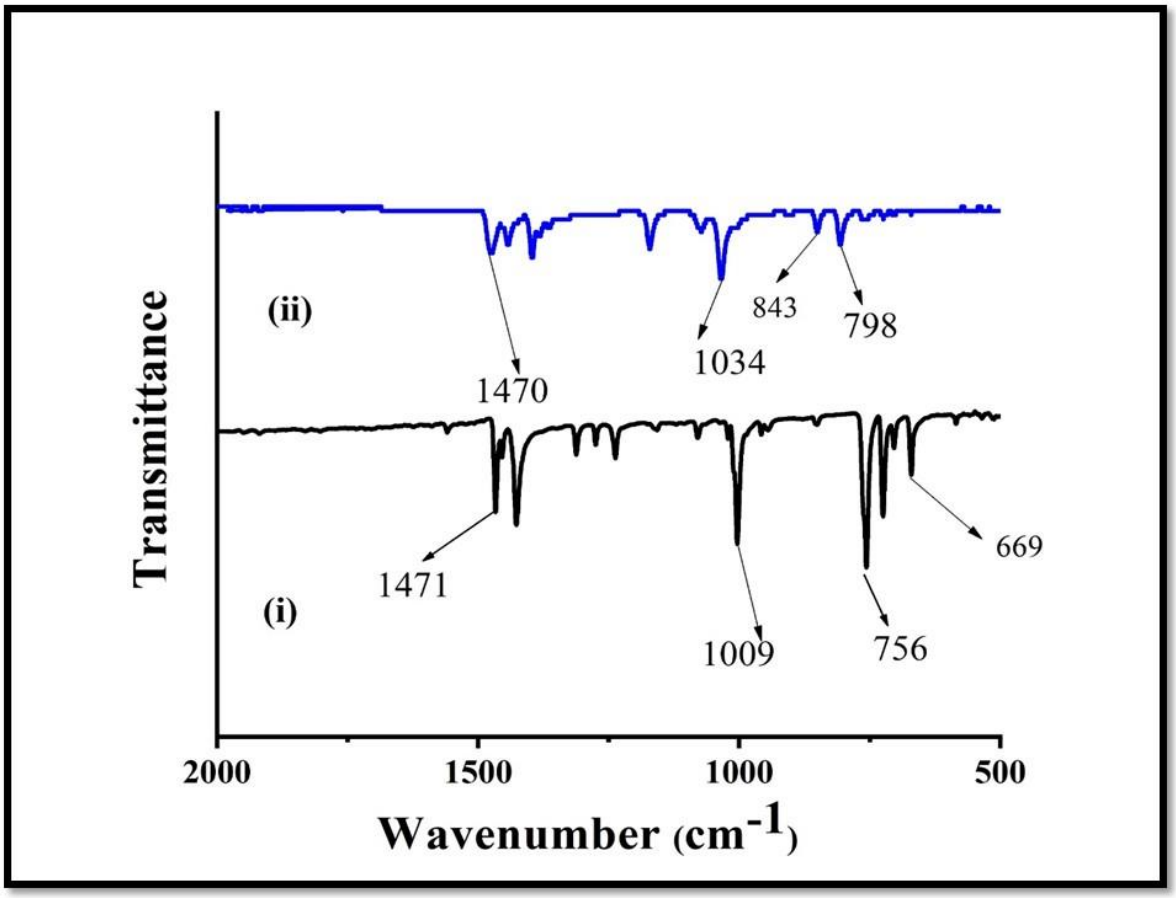

Figure 0.2: FT-IR spectra (i) uncoordinated ligand (ii) Ni-DTBTA complex

Table 3.1: IR spectra for complexes and the uncoordinated ligand

Band assignment	I	II	III
C=N	1451	1470	1471
C-N	1022	1034	1009
C=C	753	843	756
C-S	692	798	669

(I) Cd-DTBTA Complex; (II) Ni-DTBTA Complex; (III) DTBTA Ligand

3.1.2 ^{13}C Nuclear Magnetic Resonance (NMR) spectral studies of the complexes

^{13}C NMR spectroscopy is an important analytical technique used for the determination of the structures of organometallic and coordination compounds. NMR spectroscopy helps in determining the structure of the synthesized samples by use of a magnetic field (internal magnetic fields within a molecule differ distinctly at each chemical site), causing nuclei to be shielded/deshielded. The extent of shielding is influenced by many structural features within the molecule, hence the name chemical shift. Fig 3 (a) shows ^{13} C NMR spectra of Cd-DTBTA complex the complex shows six visible signals from the seven theoretically predicted signals of the uncoordinated ligand. All signals appeared between 100-160 ppm which are attributed to the chemical shift of carbon in the benzene ring and the C=C carbon character all the carbon in the benzene ring are shifted downfield , however the carbon that is bonded to the sulphur atom that is coordinated with the metal ion is shifted up field. Fig 3 (b) shows ^{13} C NMR spectra of Ni-DTBTA complex the first prominent peak at 40 ppm is the characteristic peak of DMSO . The nickel complex showed 10 visible signals shown in Table 4.2 between the ranges of 110 to 167 ppm. The was no significant change of the signals of the carbon in benzene ring however the carbon NCS_2 moiety showed a signal at around 167 ppm which is a bit higher than that of the parent ligand this confirms coordination through sulphur. The results show a relationship between the FT-IR and the NMR results the same thing was reported on literature by Rubino et al., 2017.

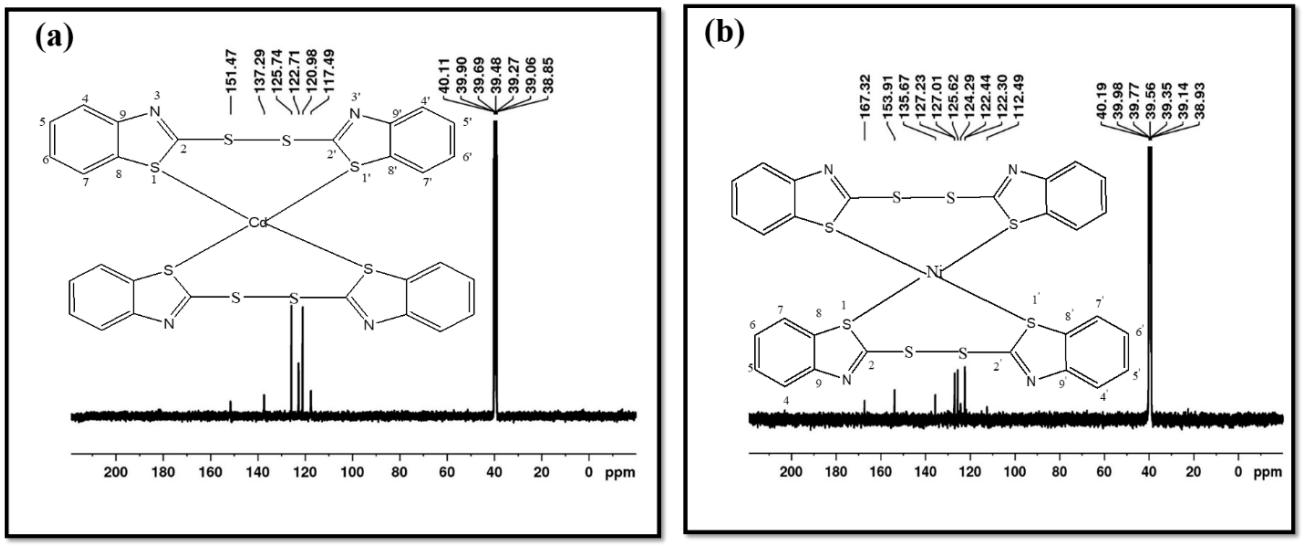

Figure 0.3: ^{13}C NMR spectra of (a) Cd-DTBTA complex and (b) Ni-DTBTA complex.

Table 3.2: NMR chemical shifts for the ligand as well as the complexes

CHEMICAL SHIFT ppm					
Ligand	C2(148)	C8,C9) 126.78	C4(125)	C7(124.36)	(C4 126.11) (C7123.17)
Complex 1	C2,C2'151,47	C8,C8' ,C9,C9' (137,29)	C4,C4'(125,47)	C7,C7'(122,71)	C5,C5',C6,C6' 120.96,117.49
Complex 2	C2,C2' 167,32,153,91	C8,C8' 135 C9(127,23),C9' (127,01)	C4,C4'(125,62)	C7,C7'(124,29) 124,44	C5C5',C6C6' 122.30,112,49

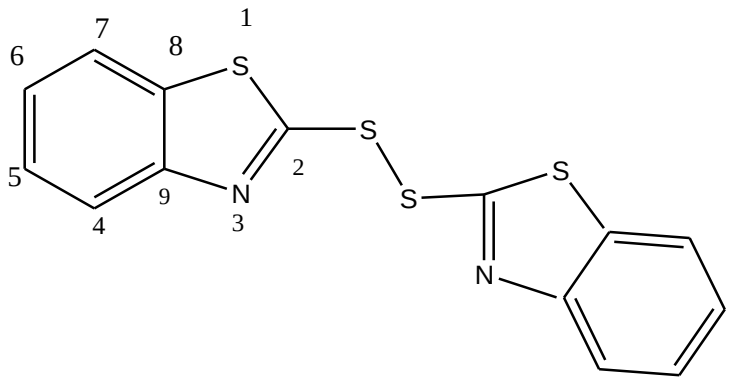

Schemes 3.3: NMR spectral numbering of the 2,2-dithiobisbenzothiazole ligand

3.1.3. Computational structural optimization

In this study theoretical calculation were attempted to study the important aspects of the prepared molecules by computational methods. In this part both the cadmium and nickel complexes have been investigated and the isomers were optimized. The molecular models of these two complexes were obtained **Fig 3.4** to display the most stable and preferred structure of the complexes. Shows the graphical presentation of the optimized structures of the different isomers with different energies (a) CdS -9948.4456808(b) NiS-4669.7315237(c)CdS -9948.4711871 and (d) NiS -4669.7210610 Ha. According to the structural models of Cd and Ni complexes have a distorted tetrahedral and square planar geometry respectively. The calculations of energy of both the complexes showed that the five membered are more stable than the seven membered ring.

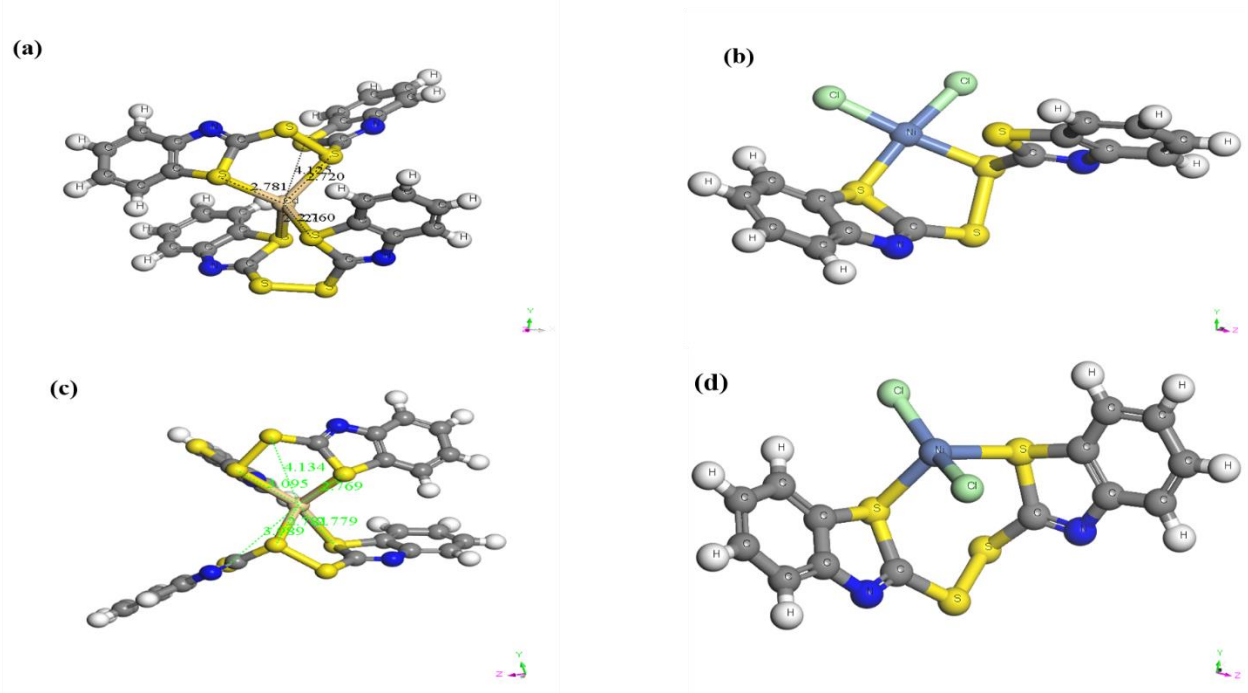

Figure 0.4: Molecular models of isomers for the prepared complexes

3.1.4. Thermal studies of the complexes

The thermal behavior of the complexes was studied under a nitrogen atmosphere from 34-900 °C. A substantial amount of reports has been based on the thermal analysis of transition metal sulphides, for both stability and their ability to produce metal sulfide products for the synthesis of nanoparticles. Thermal properties of the compounds were investigated in 20 - 900 °C temperature range at a heating rate of 10 ºC/ min under nitrogen atmosphere**. Fig 3.5** shows TGA curves for nickel and cadmium complexes. Complex I shows a single step decomposition between 238 to with a final residue 10% which is in good agreement with the theoretical value. Further more complex II also show a single step decomposition between and with a final residue of % which is in good agreement with the theoretical value of NiS (Xaba et al 2017). The thermal decomposition of all complexes was between which is within the range intended for the synthesis of the metal sulphides nanoparticles.

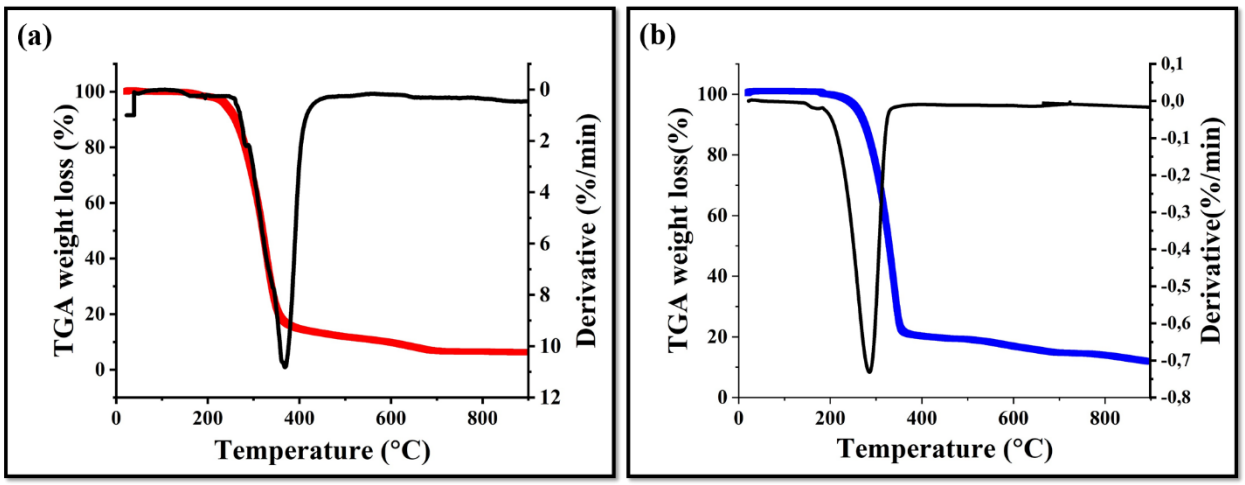

Figure 0.5: (a) TGA and DTA curves Cd-DTBTA complex (b) TGA and DTA curves Ni-DTBTA complexes.

3.2 Nanoparticles

The use of metal complexes as single source precursor for hot injection route is well established for the synthesis of nanosized materials as such particles shows size dependent optical and electrical properties. 2,2-dithiobisbenzothiazole are found to be versatile chelating ligands with the ability to form complexes with transition metal ions, as a results of their inherent metal sulphur bond. The stability of the metal complexes could be manipulated by thermolysis of the precursor compound form stable and high quality metal sulphide nanoparticles. The stability and quality of the synthesized nanoparticles not only depends on the type of the precursor used but also the capping agent / surfactant used and other parameters such as time and temperature. Capping agents (surfactant) are mainly three purposes, the first which is the main purpose is to solubilize and disperse he nanocrystals and all the reactants involved in the growth. The second is to control the metal sulphide were characterized by absorption and photoluminescence spectroscopy to determine the optical properties. XRD and TEM to study the structural properties of the nanoparticles.

3.2.1 Effect of temperature on CdS nanoparticles capped with oleylamine

3.2.1.1. Optical properties

CdS is one of the most studied semiconductor materials with the direct band gap of 2.43 eV with exciton Bohr radius of 3 nm. It is primarily used in solar cells and a variety of electronic devices.

The photoconductive and electroluminescent properties of cadmium sulphide have been applied in manufacturing of a variety of consumer goods.

(a) UV-Vis spectral studies of cadmium sulphide nanoparticles

UV-Vis spectroscopy was used to study optical properties of the nano-sized materials. The absorption spectra of the CdS nanoparticles prepared at different temperatures are shown in **Fig 3.6.** The absorption spectra of the nanoparticles synthesized at 100,150 and 200 °C exhibited band edges at 356.4, 342.0 and 323.9 nm which correspond to 3.49, 3.63 and 3.84 eV band gaps energy respectively. The increase in band gap energy is normally associated with decrease in particle size of the nanoparticles. All samples were blue shifted compared with bulk CdS which is 515 nm and band gap energy of 2.43 eV.

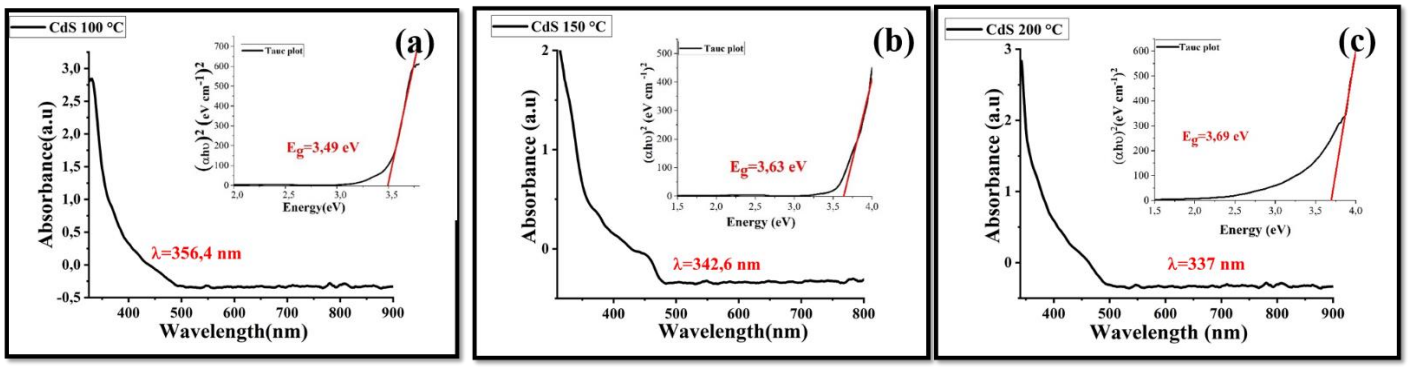

Figure 0.6: UV-VIS spectra of CdS nanoparticles prepared with 0.5 g of complex I with 6 g of OLA at (a) 100 °C, (b) 150 °(C) and 200 °C. **(Inset tauc plot)**

(b) Photoluminescence spectral analysis OLA capped nanoparticles.

Fig 3.7 shows the Photoluminescence spectra of OLA capped CdS nanoparticles the emission wavelength maxima were observed at 425 nm. It was observed that the particles prepared at high temperatures showed a narrow shape which indicates monodispersity and good passivation of the prepared nanoparticles. However it was observed for the nanoparticles prepared at low temperatures showed broad peaks which indicate agglomeration/polydispersity. Previous reports suggests that the emission arises from the recombination of an electron recombination of an electron trapped in the sulphur vacancy with a hole in the valence band of the CdS. In order to further elucidate the size and shape of the nanoparticles TEM images were studied.

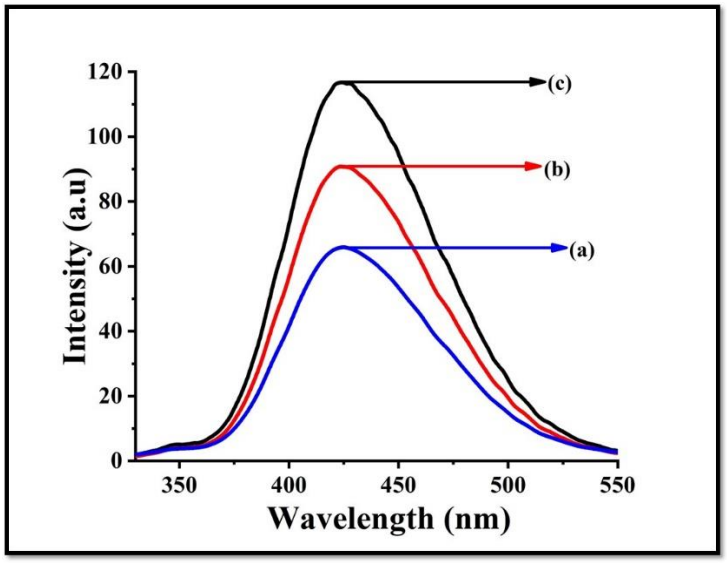

Figure 0.7: Emission spectra of CdS nanoparticles capped with OLA (a) 100 °C, 150 °C and 200 °C reaction temperature

Table 3.3: Variation of time for the preparation of CdS nanoparticles.

Reaction Temperature (°C)	Absorption bands (nm)	Emission maximum (nm)
100	356	425
150	342	425
200	377	425

3.2.1.2 Transmission Electron Microscopy (TEM).

The TEM images CdS nanoparticles prepared at different reaction temperatures are shown in **Fig 3.8**. The TEM of these nanoparticles show a decrease in particle size as the reaction temperature was increased and this can be due to the effect of decomposition rate, i.e. at high temperature, decomposition is likely to occur quickly with many nucleation sites existing simultaneously, while at lower temperature decomposition is slower, so with less nucleation sites each particle is then able to grow larger. At low 100 °C there was no distinctive shape observed however upon increase in temperature to 150 °C mini rod-like shaped nanoparticles were observed and further increase of the temperature 200 °C the shape changed to spheres and a decrease in particle size was observed. And the average particle size for the 150 and 200 °C were found to be (d) 8 nm and (e) 4 nm respectively.

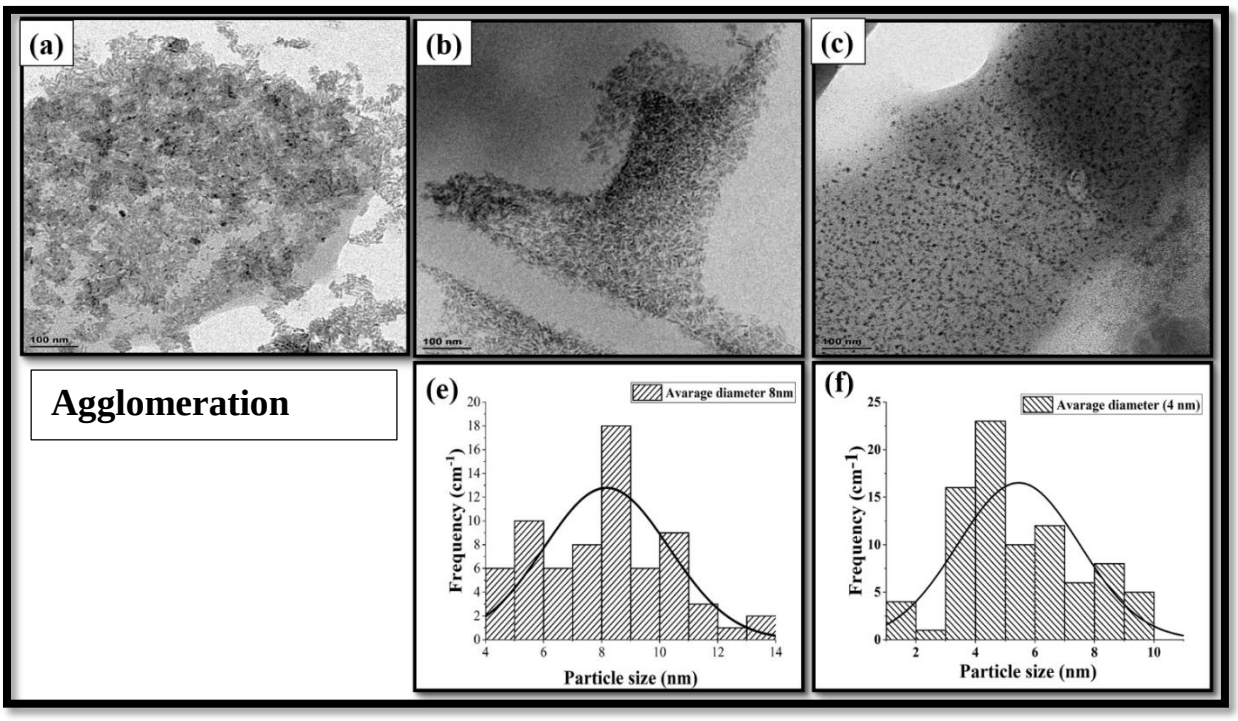

Figure 0.8 TEM micrographs of CdS nanoparticles capped with OLA at (a) 100 °C ,(b) 150 °C and (c) 200 °C and the corresponding histograms (e and f).

3.2.1.3 X-ray diffraction (XRD).

The crystalinity of the prepared CdS nanoparticles at different reaction temperatures were investigated by X-ray diffraction, as shown in **Fig 3.9 .**CdS nanoparticles have been reported to exist in two phases (cubic/hexagonal). The major diffraction peaks could be indexed as (100), (002), (101), (102), (110), and (112) of the hexagonal phase which matches with standard XRD pattern with card no: (00-002-0529). The other peaks are due oleylamine which was used as a capping agent. Although the reaction temperatures used influenced he growth of the particles but there was no visible changes in the phase of the XRD obtained in his work. It is evident that the CdS nanoparticles produced at different reaction temperatures have the same hexagonal structure. A possible explanation to this trend it may be due to the prolong heating then the resulting nanoparticles might have obtained a single phase.

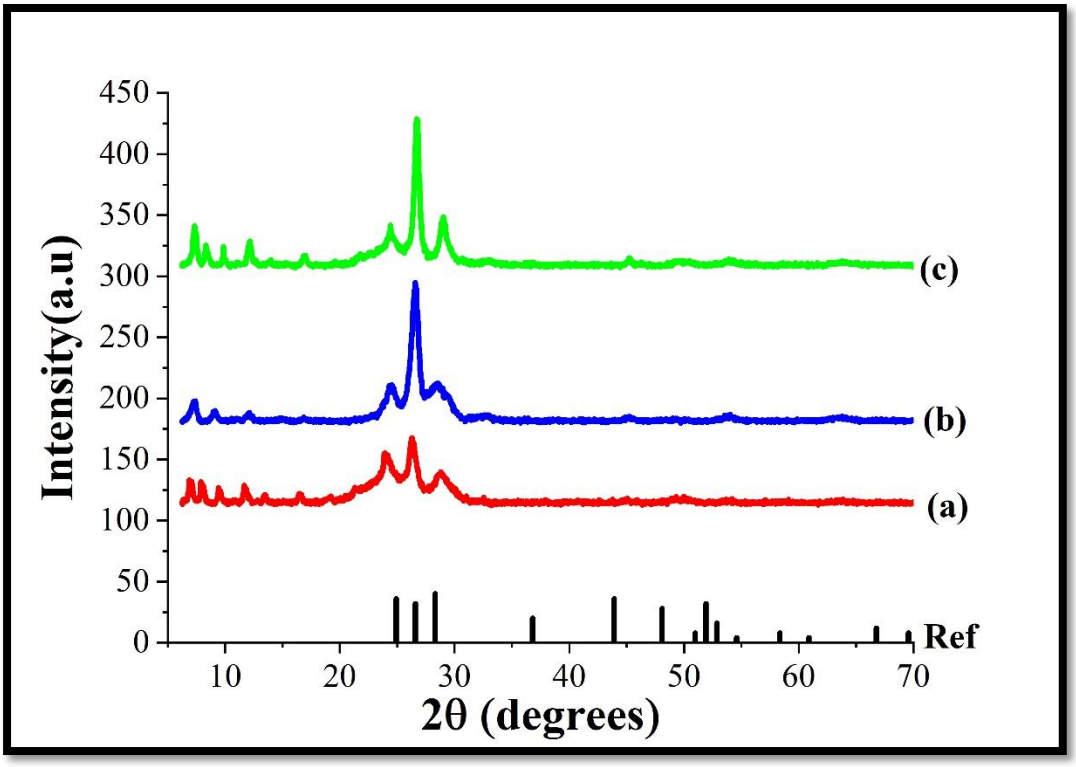

Figure 0.9: XRD patterns of CdS nanoparticles capped with OLA at (a) 100 °C, (b) 150 °C and (c) 200 °C and the corresponding reference spectra.

3.2.2 Effect of reaction time on CdS nanoparticles capped with oleylamine.

3.2.2.1 Optical properties.

(a) UV-Vis spectral studies of cadmium sulphide nanoparticles.

The variation of optical absorption as a function of wavelength for CdS nanoparticles formed at different reaction times is shown in **Fig.3.10**. The absorption band edge were found to be (323.9nm) 3.84 eV, 362.6n.m) 3.43 eV and (380.3 nm) 3.27 eV for 2hr, 2hr 30min and 3hr respectively. The absorption edges were all blue shifted from bulk CdS (515nm) 2.42 eV. Which is a clear indication of quantum size effect. However it can be observed that there is a general increase in wavelength with an increase in reaction time.

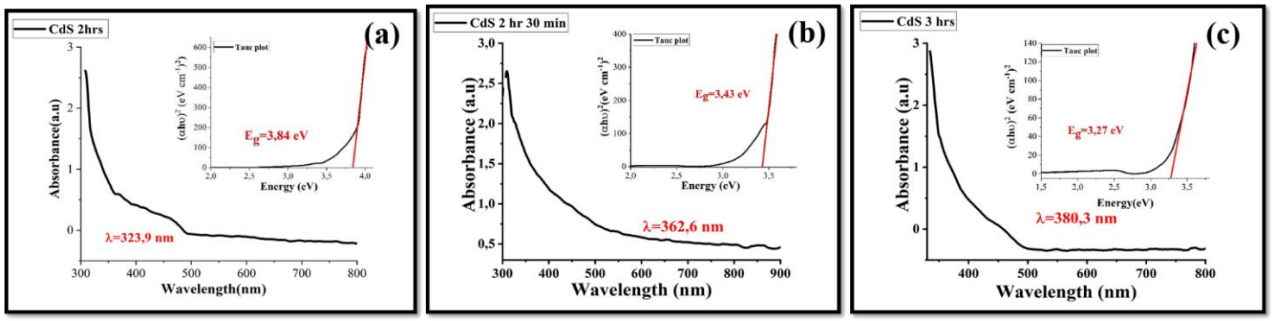

Figure 0.10: UV-Vis spectra and inset tauc plot of CdS nanoparticles prepared with 0.5 g of complex with 6 g of OLA at (a) 2 hr, (b) 2hr 30 min(C) and 3hr.

(b) Photoluminescence spectral analysis OLA capped nanoparticles.

CdS nanoparticles have frequently showed excellent photoluminescence properties generally in the visible region of the electromagnetic spectrum depending on the size of the CdS nanoparticles. **Fig 3.11** shows a typical room temperature emission spectra of CdS nanoparticles prepared by thermal decomposition methods at 200 °C. The prepared CdS nanoparticles shows a emission band edge at 426 nm at reaction time of (a) 2 hr, (b) 2hr 30 min and (c) 3hr .it was observed that all the samples emitted at the same wavelength despite different reaction times and also all the samples were red shifted from their exciton wavelength. The presence of the single peak is an indication of predominantly single morphology. The emission peaks show identical narrow shape which indicate well passivated and monodispersed nanoparticles which is also evident in TEM.

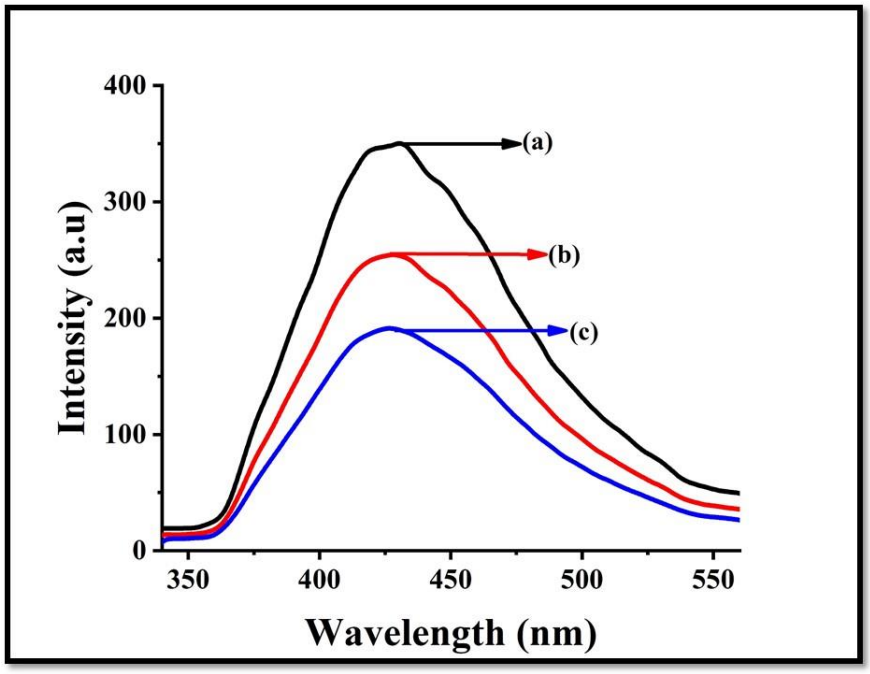

Figure 0.11: Emission spectra of CdS nanoparticles capped with OLA (a) 2hr, (b) 2hr 30 min and (c) 3 hr reaction temperature.

Table 3.4: variation of time for the preparation of CdS nanoparticles.

Reaction Time	**Absorption bands (nm)**	**Emission maximum (nm)**
2 hr	323	426
2 hr 30 min	362	426
3 hr	380	426

3.2.2.2 Transmission Electron Microscopy (TEM).

TEM images prepared from Cd-DTBTA complex capped with OLA at different reaction times are shown in **Fig 3.12** .The TEM images can depict that as the reaction time is increased the size of the nanoparticles is increased. During thermal decomposition reaction, nucleation rate for nanocrystals could reach a high value in a short time and these nuclei were wrapped by surfactant, Consequently the formed nanocrystals grows to certain value and shape (Salava-Niasari and Sobbhani 2012). For the nanoparticles prepared for (a) 2hr, (b) 2hr 30 min and (c) 3hr respectively the estimated average particle size were found to be (d) 1.5 nm, (c) 6 nm and (f) 9 nm respectively. The shape of the nanoparticles were predominantly spherical at 2hr and 2hr 30 min, however

further increase in time the particles were losing shape to form quasi spheres this is a consequence of Ostwald ripening.

In terms of kinetics, the growth of crystallite depends on the alteration of the surface energy with size. In this study two major mechanisms for the CdS nanoparticles formation were taken in consideration Ostwald's ripening and particles' aggregation. Generally the Ostwald ripening is believed to be the main path of crystal growth during precursor annealing (Antolini et al., 2011). The process corresponds to a decrease of a surface free energy when large particles developed at the expense of smaller particles. However the particles ripening is governed by temperature and time which is evident in this study.

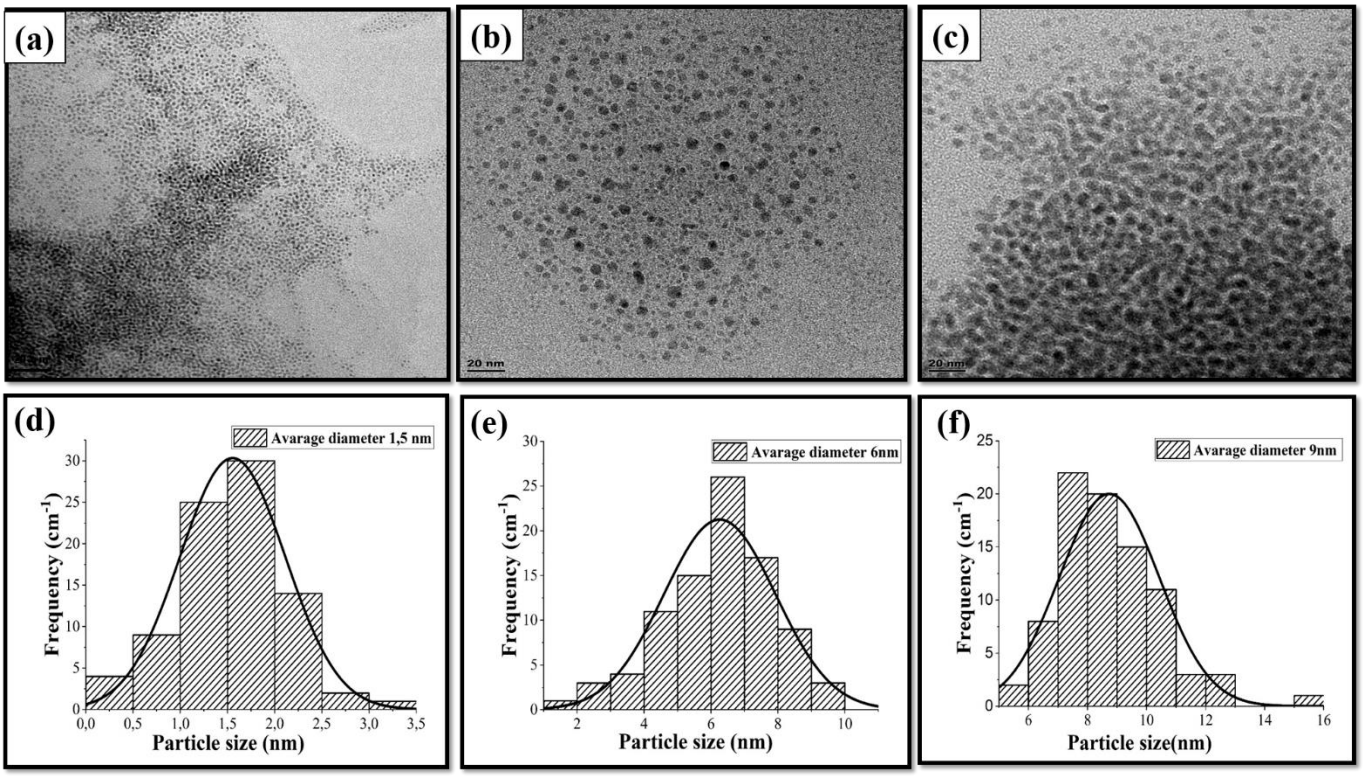

Figure 0.12: TEM micrographs of CdS nanoparticles capped with OLA at (a) 2hr, (b) 2hr 30 min and (c) 3hr and the corresponding histograms (d-f).

3.2.2.3 X-ray diffraction (XRD).

Fig 3.13 shows the XRD patterns of the nanoparticles prepared at various reaction times. The diffraction peaks correspond to (100), (002), (102) of the lattice plane and can be indexed to the hexagonal phase of CdS which matches with the standard XRD pattern (JMPD no 01-080-0006). The other unidentified peaks are due to oleylamine which was used as a capping agent .The results are in agreement with the previously reported literature (Onwudiwe et al., 2015) that the reaction time and the nature of the capping agent can influence the preferable growth directions of CdS nanoparticles, further more literature reports that the OLA capped nanoparticles are sharper than nanoparticles capped with other capping groups also indicating high crystalinity for CdS nanoparticles.

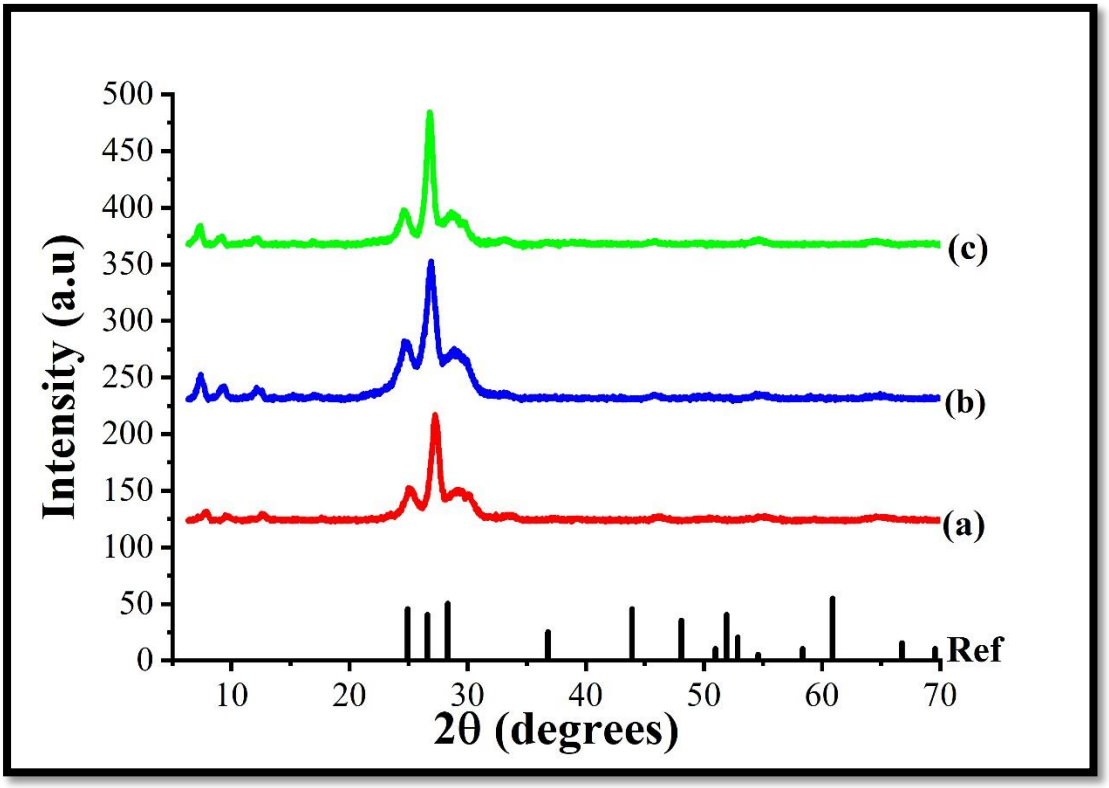

Figure 0.13: XRD pattern of Cd S nanoparticles capped with OLA at (a) 2 hr, (b) 2 hr 30 min and (c) 3 hr and the corresponding reference spectra.

3.2.3 Effect of temperature on NiS nanoparticles capped with oleylamine.

3.2.3.1 Optical properties.

Nickel sulphide is a p-type semiconductor material with a narrow band gap of 0.4 eV, most applications of nanomaterial are based on their optical properties, thus making the study optical properties very fundamental in understanding he behavior of nanoparticles .The change in the change in the size of nanoparticles can be observed by the optical properties through the shift towards higher energy (blue shift) or lower energy (red-shift) in the absorption spectra. A blue-shift is associated with the decrease in particle size due to quantum size effect and red shift is associated with the increase in particle size which is caused by aggregation of the particles. The charge carriers are separated by a distance that is known as the Bohr radius that normally has dimensions on the nanometer scale. When the size of a semiconductor material becomes similar to the Bohr radius or smaller, it leads to a situation in which the electrons and hole (excision) have a restricted space or volume to move and thus their motion is confined in all three dimensions. The decrease in particle size does not only affect the absorption spectra, the emission spectra is also affected because a change in the band gap means he change in colour and the emission of the nanoparticles

(a) UV-Vis spectral studies of nickel sulphide nanoparticles.

It has been established that temperature is a major factor which influence the particle size and growth rate of nanoparticles the effect of temperature on NiS nanoparticles capped with OLA is shown in **Fig 3.14**. The absorption band edges estimated from the spectra are 397.4 nm (3.13 eV), 350.3 nm (3.55 eV) and 345.5 nm (3.60 eV) for 100, 150 and 200 °C respectively. It was observed that there was a systematic shift to smaller wavelength on the absorption edge of the nanoparticles. This is due to the quantum confinement effect where more discrete energy states are formed.

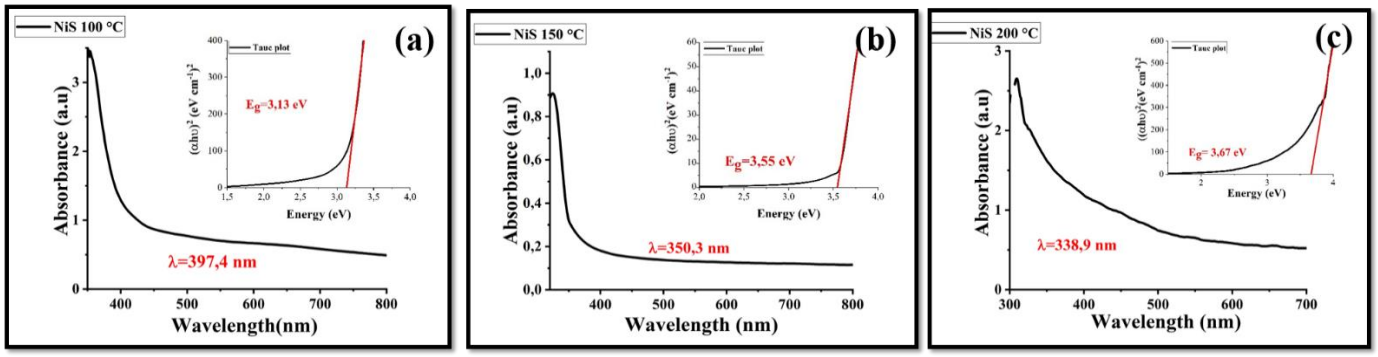

Figure 0.14: UV-VIS spectra and inset tauc plot of NiS nanoparticles prepared with 0.5 g of complex I with 6 g of OLA at (a) 100 °C, (b) 150 °C and (c) 200 °C.

(b) Photoluminescence spectral analysis of OLA capped nanoparticles.

The emission spectra of the nickel sulphide nanoparticles synthesized at different temperatures from Ni-DTBTA complex is shown in **Fig 3.15 (a-c)**. The photoluminescence spectra were observed with a strong emission peak at (a) 336 nm, (b) 337 nm and (c) 338 nm respectively (Table 5.3) when excited at 400 nm. The emission peaks were all red shifted in relation absorption peaks .The broad emission peaks at low temperature are an indication of broader size distribution shown by distribution curves this was further confirmed by TEM. The emission maxima slightly shifted to low wavelength as the temperature was increased. This indicates that the nanoparticles were getting smaller with an increase in temperature.

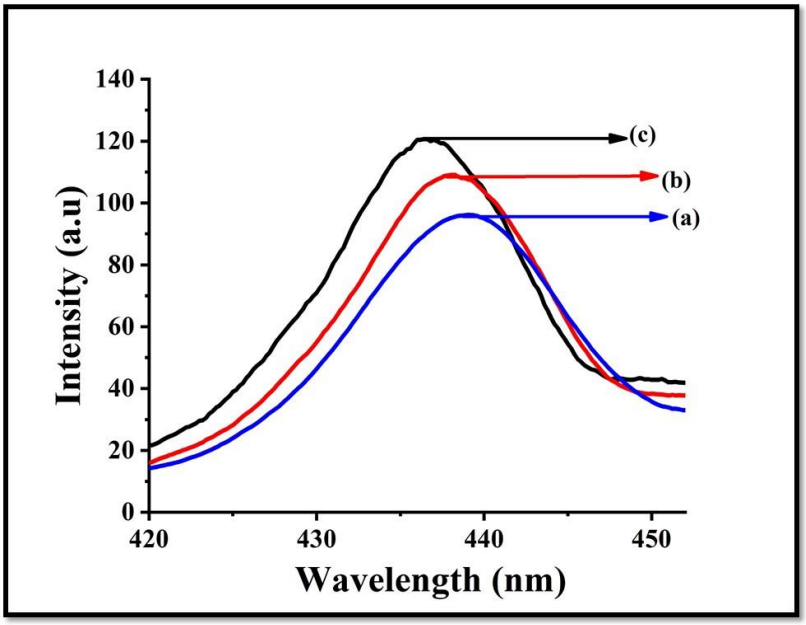

Figure 0.15: Emission spectra of NiS nanoparticles capped with OLA (a) 100 °C, (b) 150 °C and (c) 200 °C reaction temperature.

Table 3.5: Variation of temperature for the preparation of NiS nanoparticles.

Reaction Temperature (°C)	Absorption bands (nm)	Emission maximum (nm)
100	397	438
150	350	437
200	338	436

3.2.3.2 Transmission Electron Microscopy (TEM).

TEM was used to study the effect of temperature on the size and shape of NiS nanoparticles **Fig 3.16** shows the TEM images of NiS NP's capped with OLA synthesized at different reaction temperatures. It was observed that at low temperature the particles didn't have any distinct shape however upon increase in temperature to 150°C resulted in the formation of spherical nanoparticles, further increase of the temperature to 200 °C spherical particles with uniform shape were observed with average diameter of 7 nm. It was observed that nanoparticles synthesized at high temperature favored thermodynamic growth regime similar results were reported by Thangwane and co-workers.

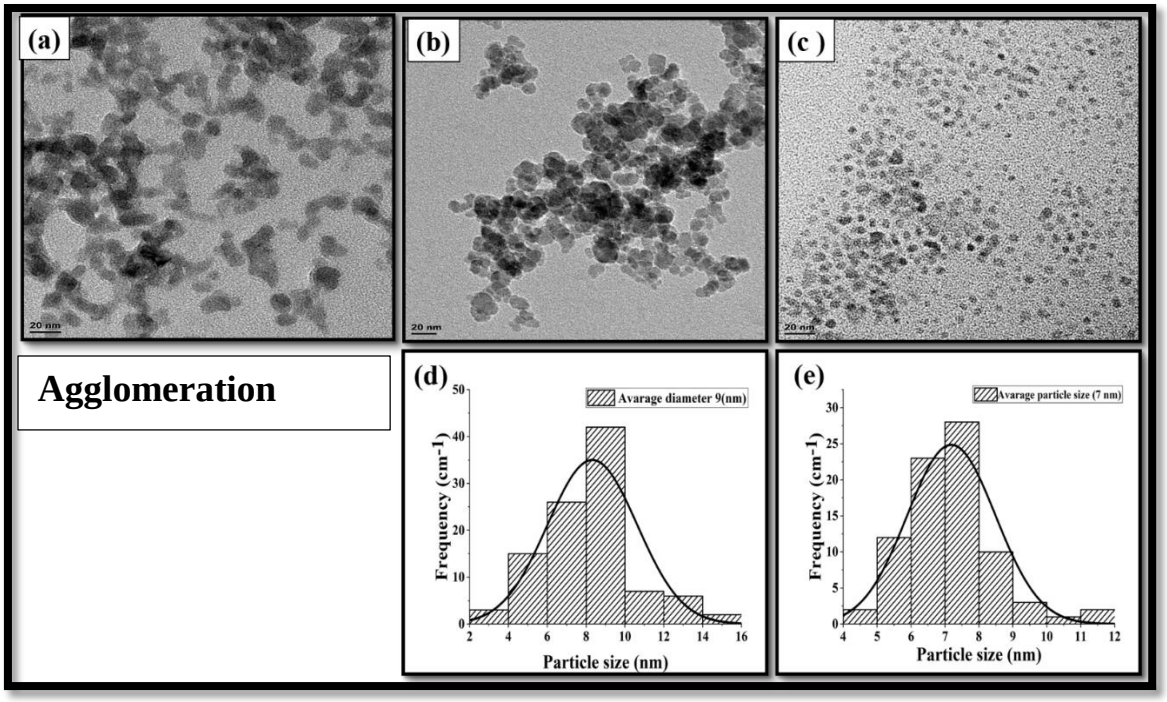

Figure 0.16: TEM micrographs of NiS nanoparticles capped with OLA at (a) 100 °C, (b) 150 °C and (c) 200 °C and their corresponding histogram (d and e).

3.2.3.3 X-ray diffraction Spectroscopy.

The powder X-ray diffraction patterns of the NiS nanoparticles synthesized at different temperatures is shown in **Fig 3.17** the XRD pattern of the NiS nanoparticles prepared at 100 °C shows one amorphous peak at 2θ value 22.7° which corresponds to 220 miller indices for orthorhombic (Ni_7S_6) crystalline phase with (JCPCD card no. 01-077-3507). for the nanoparticles prepared at 150 °C the XRD patterns show four major peaks at 2θ values of 19.4° ,32.0° ,40.4° and 52.18° which correspond to (110), (300),(211) and (401) miller indices for rhombohedral (βNiS millerite) crystalline phase with (JCPCD card no. 01-074-7239) and the nanoparticles prepared at 200 °C the XRD patterns shows four major peaks at 2θ values 30.1 °,34.6°,45.9 °,53 ° which correspond to (100), (101), (102) and (110) miller indices and it was indexed to hexagonal (αNiS) crystalline phase. The change in reaction temperature had a significant change in the crystalline phase of the nanoparticles (Shombe et al., 2020) observed similar results.

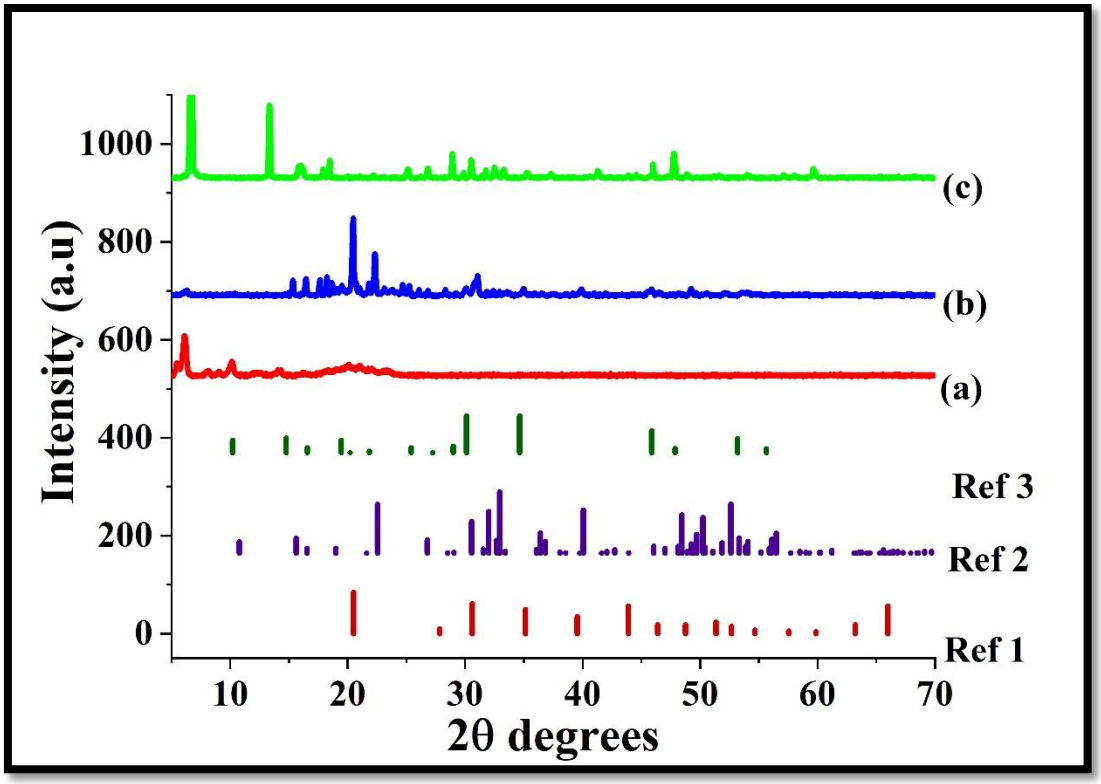

Figure 0.17: XRD patterns of NiS nanoparticles capped with OLA at (a) 100 °C, (b) 150 °C and (c) 200 °C and the corresponding reference spectra's.

3.2.4. Effect of reaction time on NiS nanoparticles capped with oleylamine.

3.2.4.1 Optical properties.

(a) UV-Vis spectral studies of nickel sulphide nanoparticles.

UV-Vis spectral analysis has been widely used to characterise semiconductor nanoparticles. As the particles size decreases the absorption edge shifts to shorter wavelength, due to the band gap increase of the smaller particles. The absorption bands are blue shifted from the bulk NiS which is an indication of quantum size effect. The absorption spectra of the NiS nanoparticles synthesized at different reaction times are shown in **Fig 3.18 (a-c).** The absorption bands and their resulting band gap energy were observed at (a) 345.5 nm (3.60 eV), (b) 354.3 (3.51 eV) nm and (c) 391.1 (3.18 eV) nm respectively (Table 5.4). These spectra indicated that there was an increase in the particle size with an increase in time and this is confirmed by PL and TEM.

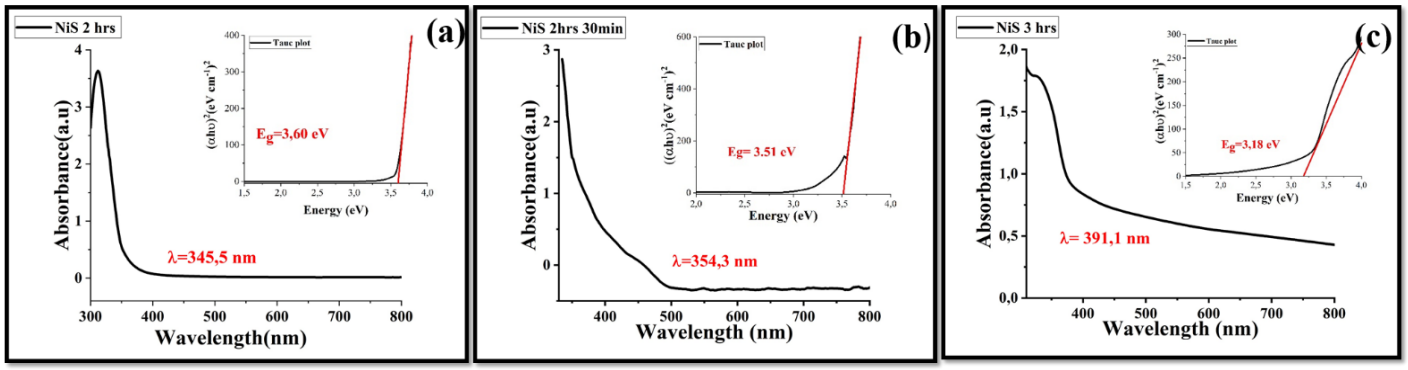

Figure 0.18: UV-Vis spectra and inset tauc plot of NiS nanoparticles prepared with 0.5 g of complex with 6 g of OLA at (a) 2 hr, (b) 2 hr 30 min (C) and 3hr.

(b) Photoluminescence spectral analysis of OLA capped NiS nanoparticles.

The emission spectra for the nickel sulphide nanoparticles synthesized at different reaction times from Ni-DTBTA complex is shown in **Fig 3.19**. The entire spectra show one major emission peak. The emission peaks are red shifted in relation to the absorption peaks the corresponding photoluminescence spectra were observed with a strong emission peaks centered 537 nm when excited at 400 nm .The sharp emission peaks observed are indicative of a narrow size distribution and this was confirmed by distribution curves. As the reaction time was increased the emission peaks broadens and this shows that the particle size is getting bigger.

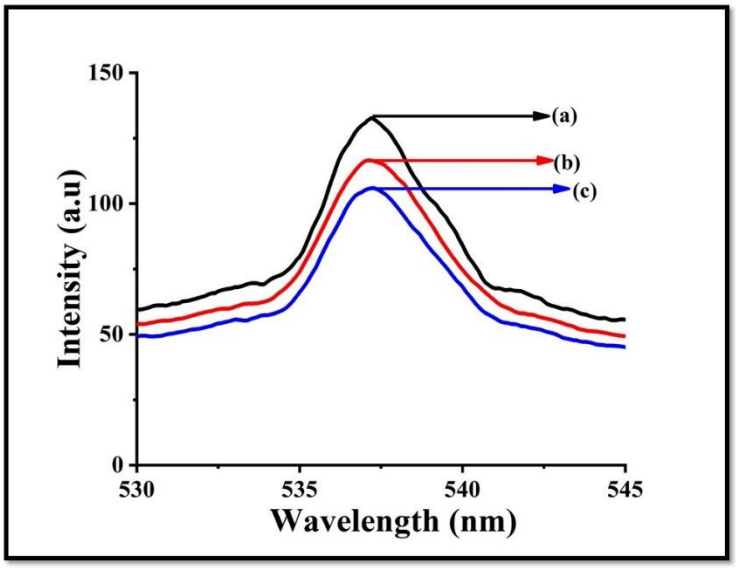

Figure 0.19: Emission spectra of NiS nanoparticles capped with OLA (a) 2hr, 2 hr 30min and 3 hr reaction time.

Table 3.6: Variation of time for the preparation of NiS nanoparticles.

Reaction Time	**Absorption bands (nm)**	**Emission maximum (nm)**
2 hr	345	537
2hr 30 min	354	537
3 hr	391	537

3.2.4.2 Transmission Electron Microscopy (TEM)

TEM images prepared from Ni-DTBTA complex capped with OLA at different reaction times are shown in **Fig 3.20**. The TEM images can depict that as the reaction time is increased the size of the nanoparticles is increased. For the nanoparticles prepared for (a) 2 hr, (b) 2hr 30 min and (c) 3hr respectively the estimated average particle size were found to be (d) 6 nm (e) 12 nm. The shape of the nanoparticles were predominantly spherical at 2 hr and 2 hr 30 min, however further increase in time the particles were losing shape to form agglomerated particles this is a consequence of Ostwald ripening.

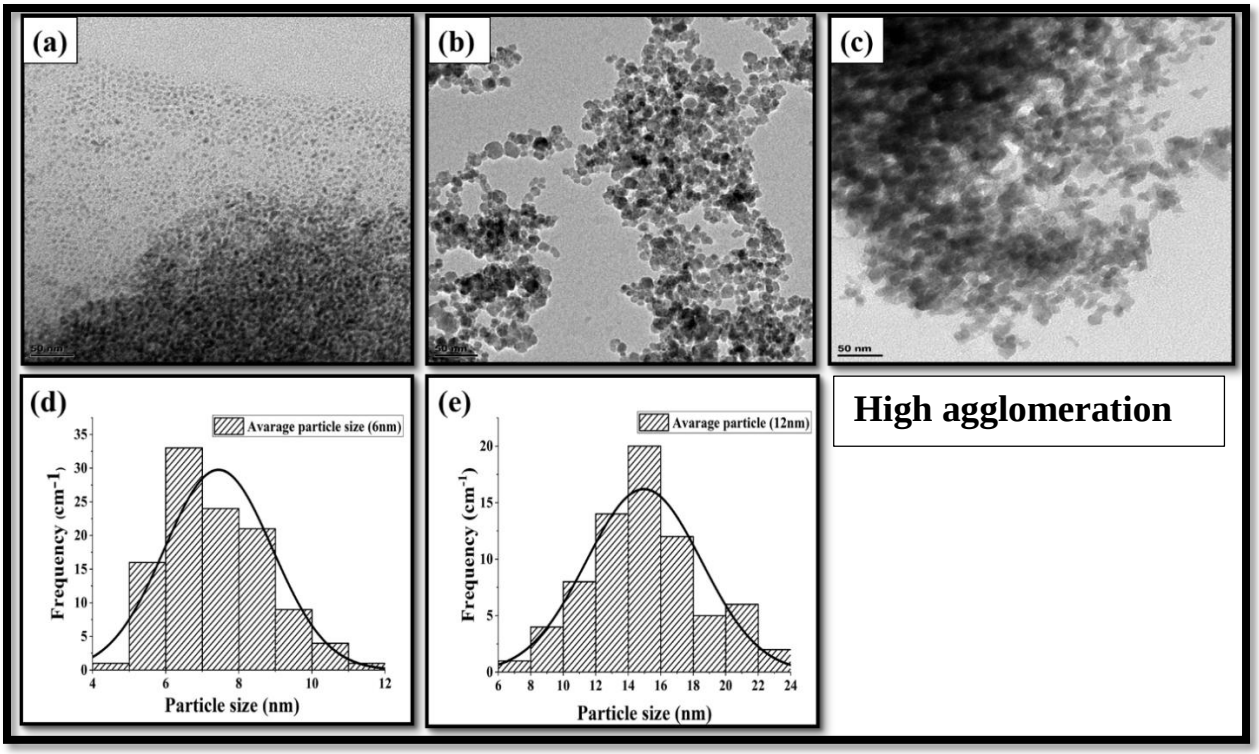

Figure 0.20: TEM micrographs of NiS nanoparticles capped with OLA at (a) 2 hr, (b) 2hr 30 min and (c) 3hr and the corresponding histograms (d-e).

3.2.4.3 X-ray diffraction (XRD).

The XRD pattern of NiS nanoparticles prepared at different reaction times is shown in **Fig 3.21.** The XRD pattern at 2 hours shows two major peaks at 2θ of 30.2° and 34.4° which correspond to (100) and (101) miller indices for orthorhombic (Ni_6S_5) crystalline phase with (JCPDS file card no. 01-082-7451) , the nanoparticles prepared at 2 hours and 30 minutes showed four major peaks at 2θ values of 30.2, 34.4, 46.0 and 53.8 which correspond to (100), (101),(102) and (110) miller indices for orthorhombic (Ni_6S_5) crystalline phase with (JCPDS file card no. 01-082-7451) and the XRD pattern of the nanoparticles synthesized at 3 hours there were four major peaks observed at 2θ value of 27.5°, 31.8°, 35.5° and 45.5° which correspond to (111), (200)(210) and (220) miller indices with cubic (Vaesite NiS) crystalline phase with (JCPDS card no 00-003-0734). These results showed that the variation in reaction time had a significant change on the crystalline phase of the prepared nanoparticles with the crystalinity increasing with prolong reaction time.

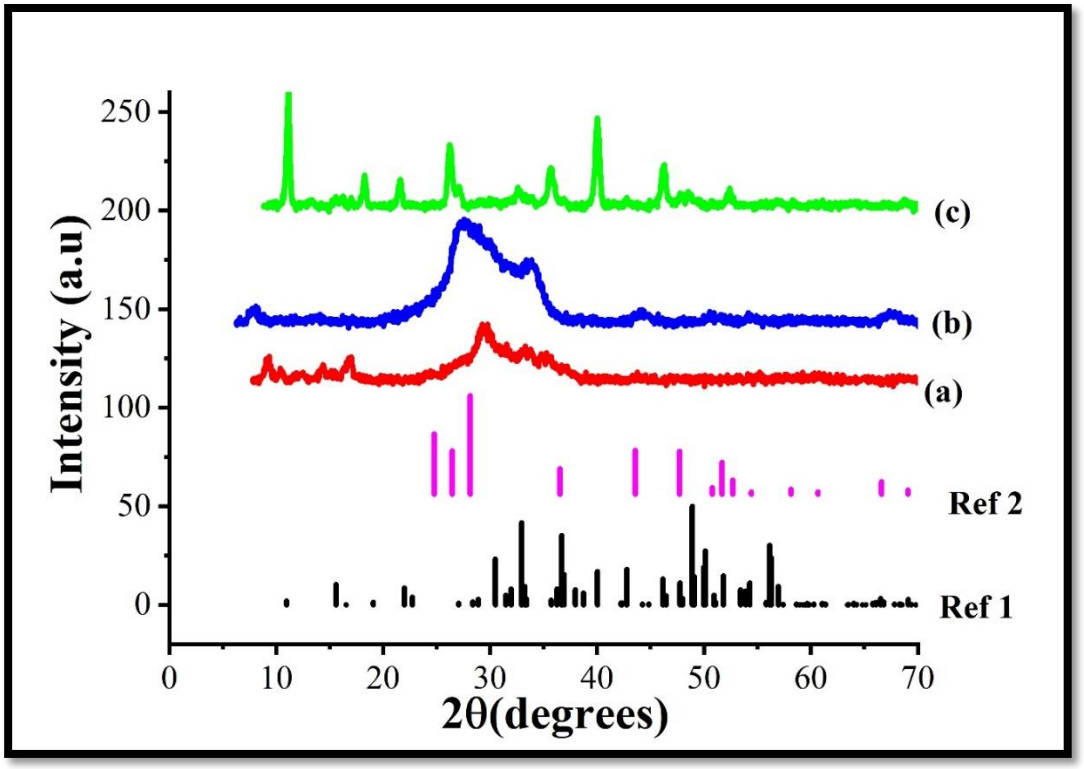

Figure 0.21: XRD patterns of NiS nanoparticles capped with OLA at (a) 2 hr, (b) 2 hr 30 min and (c) 3hr and the corresponding reference spectra.

3.3 ELECTROCHEMICAL METHODS.

The overall aim of this work is to synthesize CdS and NiS based nanomaterials the optimum time and temperature were then explored for their applications in electrochemical sensors for the determination of Rhodamine B dye. Electrochemical sensor are a suitable tool for rapid and sensitive analysis with wide range of applications. For the last two decades modified electrodes have been used as sensors for electrochemical detection of various organic dyes like Rhodamine B, Brilliant green and methyl orange. Modification of electrodes to attain high sensitivity, selectivity and compatibility necessitates extensive study. The excellent performance of modified electrode depends upon various modifiers such as carbon materials, conducting polymers and metal nanoparticles. Current research for new emerging electrode materials is now focused on semiconductor metal sulphide nanoparticles.

3.3.1 Electrochemical characterization.

3.3.1.1 Cyclic Voltammetry (CV) and electrochemical impedance spectroscopy (EIS).

Electrochemical Impedance Spectroscopy (EIS) is an effective tool for studying the interface properties of the unmodified and modified electrodes. The resistance to charge transfer is the be estimated from the the high frequency semi-circular part of the Nyquist plot in the EIS most significant indicator for the electrochemical property among other impedence . The larger the diameter of the semi-circularpart the larger corresponding resistance of charge transfer. The low-frequency linear part of the Nyquist plot is related to the diffusion control process is the most significant indicator frequency semi-circular part of the Nyquist curve in EIS.

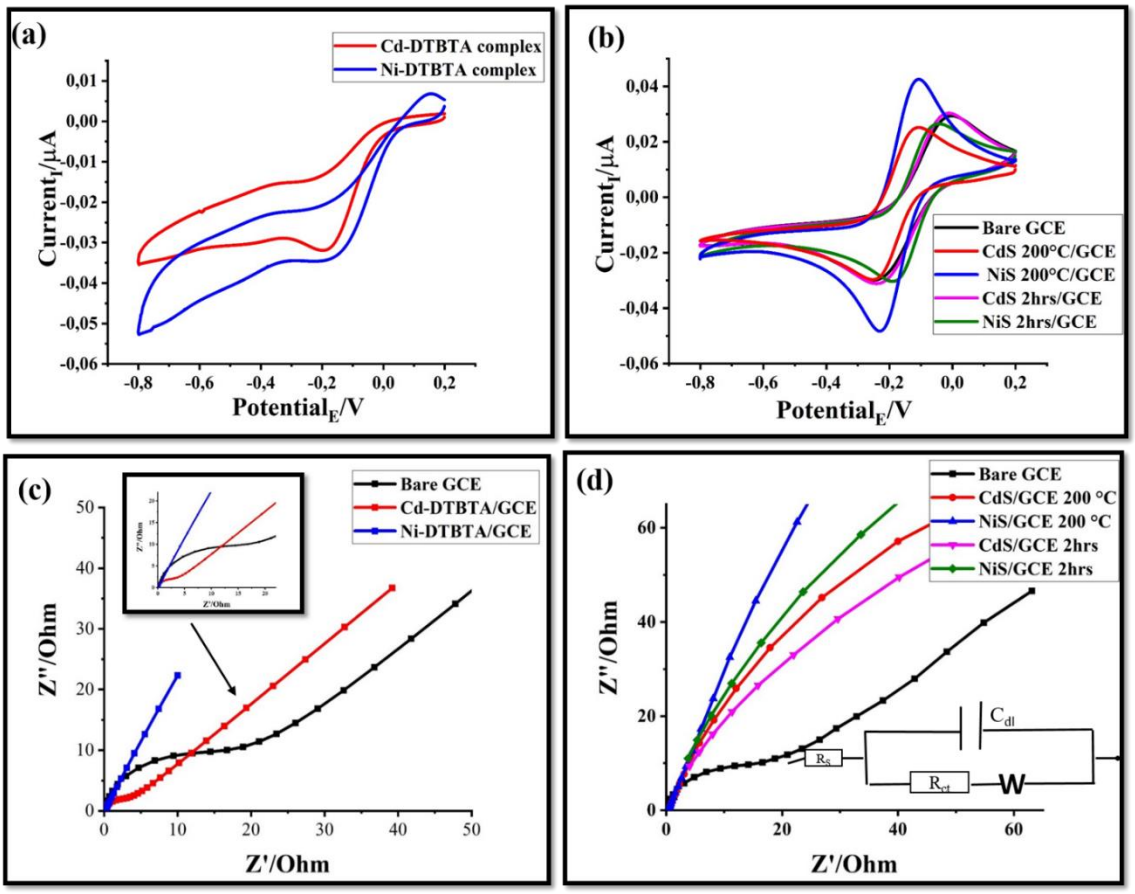

Figure 0.22: The EIS Nyquist plot of $K_3[Fe(CN)_6]$ (25 mM containing 0.1 M KCl) of (a) Bare GCE, Cd-DTBTA/GCE, Ni-DTBTA/GCE Bare GCE, CdS/GCE@ 2 hr, NiS/GCE @ 2 hr, CdS/GCE @ 200 °C, NiS/GCE @ 200 °C

Fig 3.22 (c) revealed an over lay of Nyquist for the different complexes electrodes using the redox couple $K_3[Fe(CN)_6]$ solution contaimg 0.1 M KCl. The EIS at the bare GCE had an obvious semicircle while the diameter of the semicicle is decreased in both the Ni-DTBTA/GCE and Cd-DTBTA/GCE once the electrode is modified.The difference in semicircular portion at different electrodes implies that Ni-DTBTA exhibit a low resistance to charge and high electron transfer rate than the Cd-DTBTA because Nickel sulphides are known to have high stability and well defined redox properterties due to the metal-ligand charge transfer, ligand metal charge transfer or intervalence charge transfer of nickel sulphides. **Fig 3.22(d)** revealed an overlay of the nanopartcles modified electrodes the EIS of the nanopartcles shows a decrease in the diameter of the semicircle this is due the high stability , rich active sites for the reaction , high surface area and good electron conductivity .Moreover the NiS/GCE @ 200 °C exhibit very low restistance of charge transfer this suggest that NiS/GCE @ 200 °C improves the charge transfer efficeincy and this also suggest that there is an increase in the electron transfer rate due to the nanodructured property of NiS.Therefore the performance of the nanostructured materials will be explored for eletrochemical determination of Rhoamine B.

Table 3.7 : electron transfer rate values for the different modified elecrodes.

Electrode	**R_{ct} Value (Ohm)**
BARE	16 058
Cd-DTBTA	2710
Ni-DTBTA	170,6
CdS/GCE 200 °C	125
NiS/GCE 200 °C	52
CdS/GCE 2 hr	140
NiS/GCE 2 hr	100

3.3.2 Electrochemical behavior

3.3.2.1 Differential pulse voltammetry (DPV)

Electrochemical behaviour of RhB at different electrodes were investigated differential pulse voltammetry (DPV) to demostrate the signal amplification of the modified CGE at pH 7, **Fig.3.23 (a)** shows a pronounced and wide peak at the bare GCE, as the electrode was futher modified by Cd-DTBTA a weak oxidation peak was observed at the Cd-DTBTA electrode which suggest that Cd-DTBTA had a low electrocatalytic activity than the unmodifed electrode . The oxidation peak current at Ni-DTBTA was 0.9 times larger than that of Cd-DTBTA complex these observations suggested that oxidation peak current at Ni-DBTA/GCE exhibit better efficiency because of the stability of nickel than that of cadmium **Fig. 3.23 (b)** the electrochemical behaviour of RhB at the NiSNPs/GCE and CdSNPs/GCE synthesized at Different parameters, the bare GCE is relatively low which indicates that the oxidation activiity of RhB is weak on the bare GCE surface. When the surface is modified oxidation signal of RhB increases. NiS nanoparticles have excellent electrocatalytic activity and electrical conductivity. Hence the large oxidation peak current was obtained at NiS/GCE synthesized at 200 °C. The above results could be attributed to that the nanoparticles at 200 °C is evenly dispersed since the dpv has a better resolution . NiS nanoparticles are more efficient and has exhibited enhanced funtional properties than the complexes it is clear that the nickel sulphide nanopartcles display strong enhancement effect on the oxidation of RhB this is shown by a remakable peak current increase. Modification of the electrode with NiS nanoparticles increases the surface roughness and consequently provides larger responses area which results in much higher accumulation efficiency for RhB.

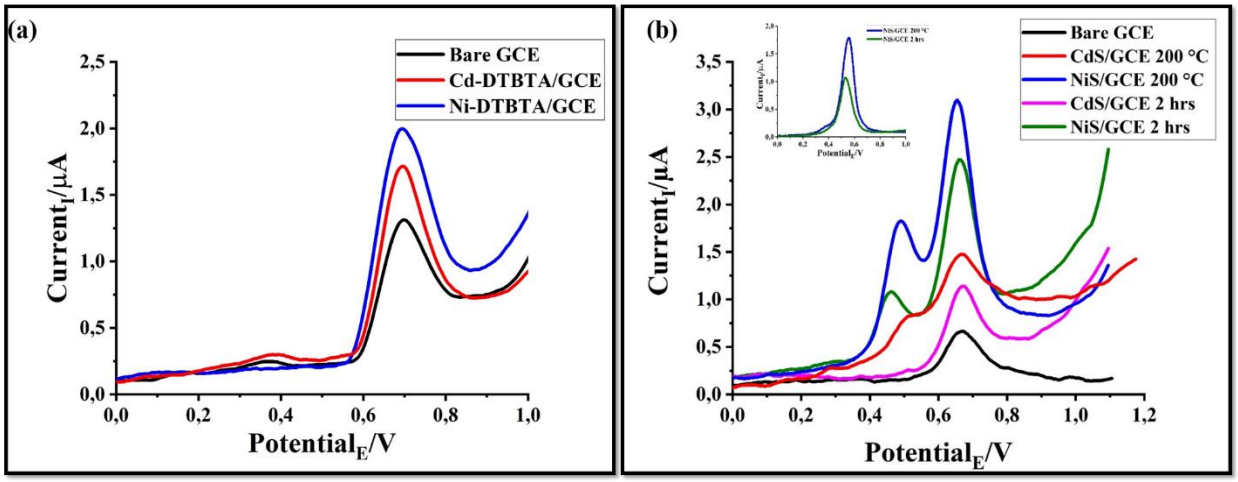

Figure 0.23: Differential pulse voltammograms of Bare GCE, Cd-DTBTA/GCE, Ni-DTBTA/GCE (a) Bare GCE, CdS/GCE@ 2 hr, NiS/GCE @ 2 hr, CdS/GCE @ 200 °C, NiS/GCE @ 200 °C(b) in 0.1 M PBS solution at pH 7 containing 1 mM RhB.

3.3.3 Method development for electrochemical detection of Rhodamine B using the optimum complexes and nanoparticles

3.3.3.1 Effect of pH

The effect of acidic and neutral pH on the electrochemical behavior of RhB were studied at the pH range of 3 - 8. The response current increase linearly with an increase in pH as shown in **Fig 3.24 (a)**. The oxidation peak currents reach the maximum value at pH 7. The pH 7 was chosen as the optimal pH for the detection of RhB at Ni-DBTA/GCE. **Fig 3.24 (b)** shows the effect of pH on the current response of the NiS/GCE @200 °C. This effect was studied using DPV at NiS/GCE @200 °C to measure RhB (0.1 M phosphate buffer) at pH range of 2 to 8. The voltammograms showed two well-defined shaped oxidation peak current at pH 8, showing a clear influence of the pH on the electrochemical oxidation of RhB at the NiS/GCE @ 200 °C surface. Thus a phosphate buffer solution of pH 8 was used further for the subsequent experiments in this work.

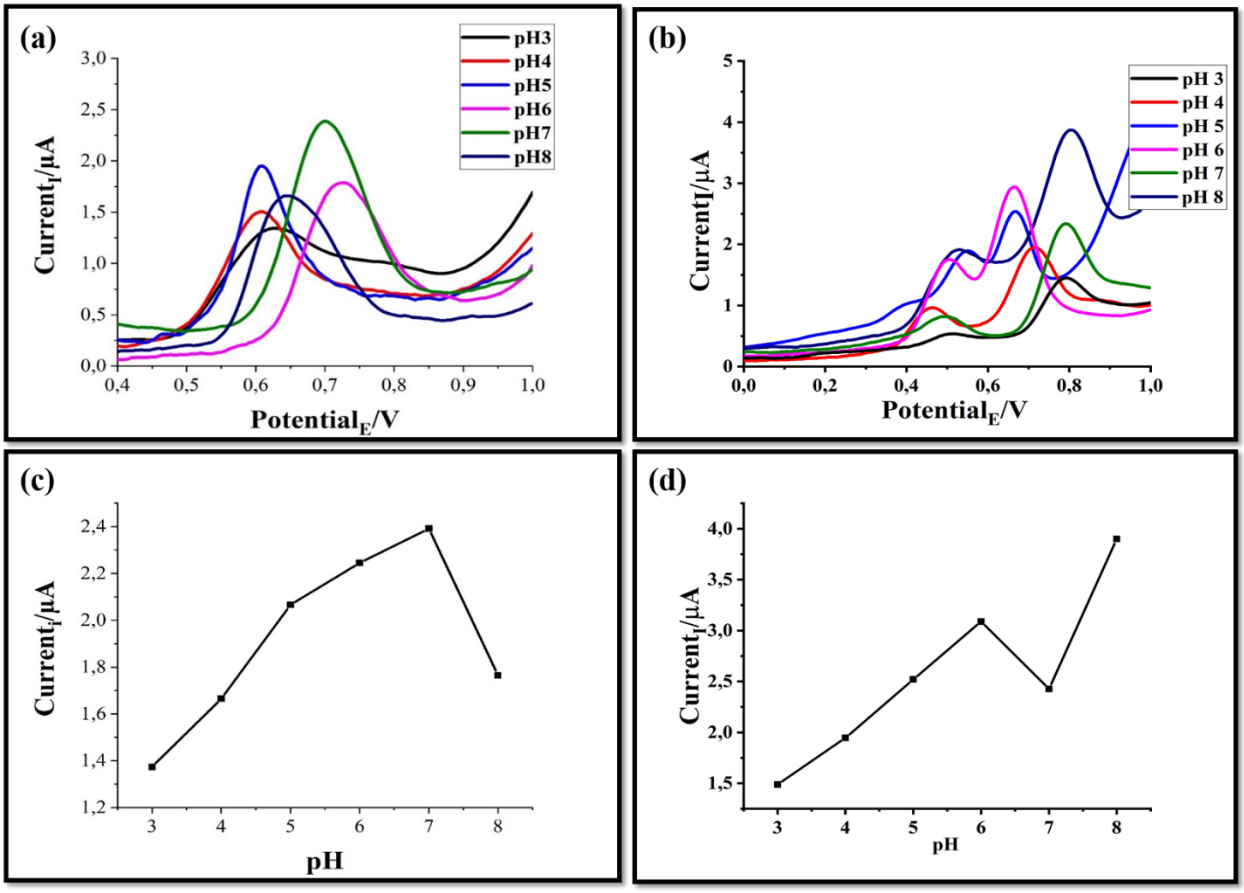

Figure 0.24 : Differential pulse voltammograms of 1mM RhB in 0.1 M PBS solution at pH different (3,4,5,6, 7 and 8) for Ni-DTBTA/GCE (a) for NiS/GCE @ 200 °C (b)the relationship between peak current and pH (c) Ni-DTBTA (d) NiS/GCE @200 °C.

3.3.3.2 Effect of concentration

Differential Pulse voltammetry was used to investigate the effect of increasing concentrations of RhB on the Ni-DBTA/GCE shown in **Fig.3.25 (a)**. The DPV results were used for the determination of the limit of detection (LOD) and the linear range of the modified electrode. The increase in RhB concentration was studied in the range of 0.02-1.0 Mm. The increase in RhB concentration produced a proportional increase in the peak current on the surface of the Ni-DBTA/GCE. The graph of I_p against concentration was plotted which showed a straight line with good linearity was shown in **Fig. 3.25(c)** the correlation coefficient value was found to be 0.9938 and the limit of detection (LOD) which was defined as (3S/M) where S is the standard deviation of the blank and M is the Slope was calculated to be 4.87 mM for the Ni-DTBTA/GCE. The peak current increase with an increase of concentration from 0.01-0.06mM as shown in **Fig.3.25(b) and**

Fig 3.25 (d). The detection limit was estimated to be as 2.75 nM with the R^2=0.9904. Compared with other electrochemical sensors, the NiS/GCE @ 200°C exhibited relatively high sensitivity with a wide linear range.

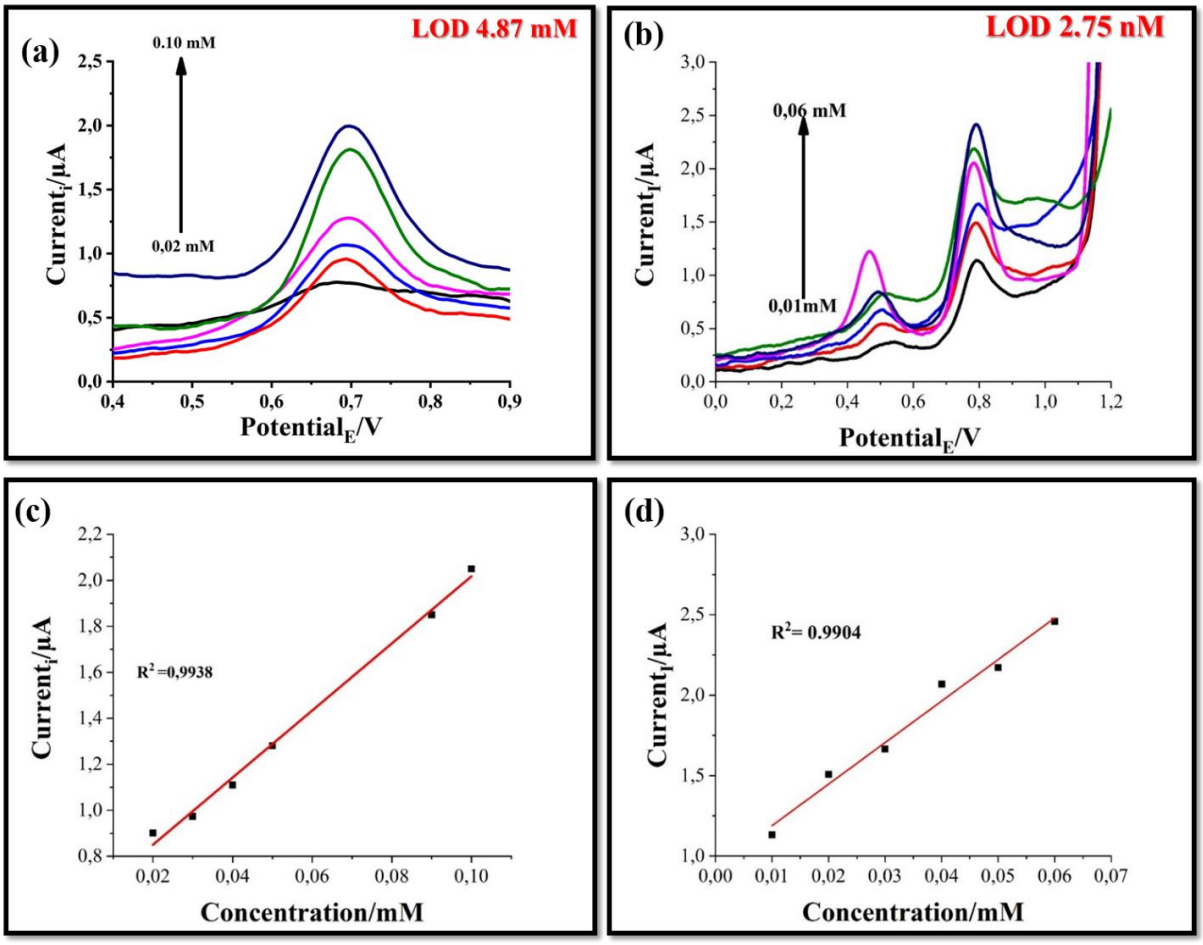

Figure 0.25: Differential pulse voltammograms of 1mM RhB in 0.1 M PBS solution at different concentration (0.02,0.03,0.04,0.05 and 0.10) for Ni-DTBTA/GCE (a) (0.01,0.02,0.03,0.04,0.05,0 and0.06) for NiS/GCE @ 200 °C (b)the relationship between peak current and concentration (c) Ni-DTBTA (d) NiS/GCE @200 °C.

3.3.3.3 Reproducibility and repeatability studies

The reproducibility of RhB determination by Ni-DTBTA/GCE **Fig 3.26 (a)** was investigated by using DPV. The determination of 0.04 mM RhB done by using two independently produced electrodes, the electrodes were used to measure 2 different samples of 0.04 mM RhB .The

oxidation current produced by the two samples replicates independently determined by the two electrodes and they gave a relative standard deviation of 0.5%. Hence showing good reproducibility. The repeatability of the method was also investigated by using the modified electrodes for all two determination of 0.04 mM RhB. The relative standard deviation of the measured peak current was found to 4% be showing good repeatability of the method.

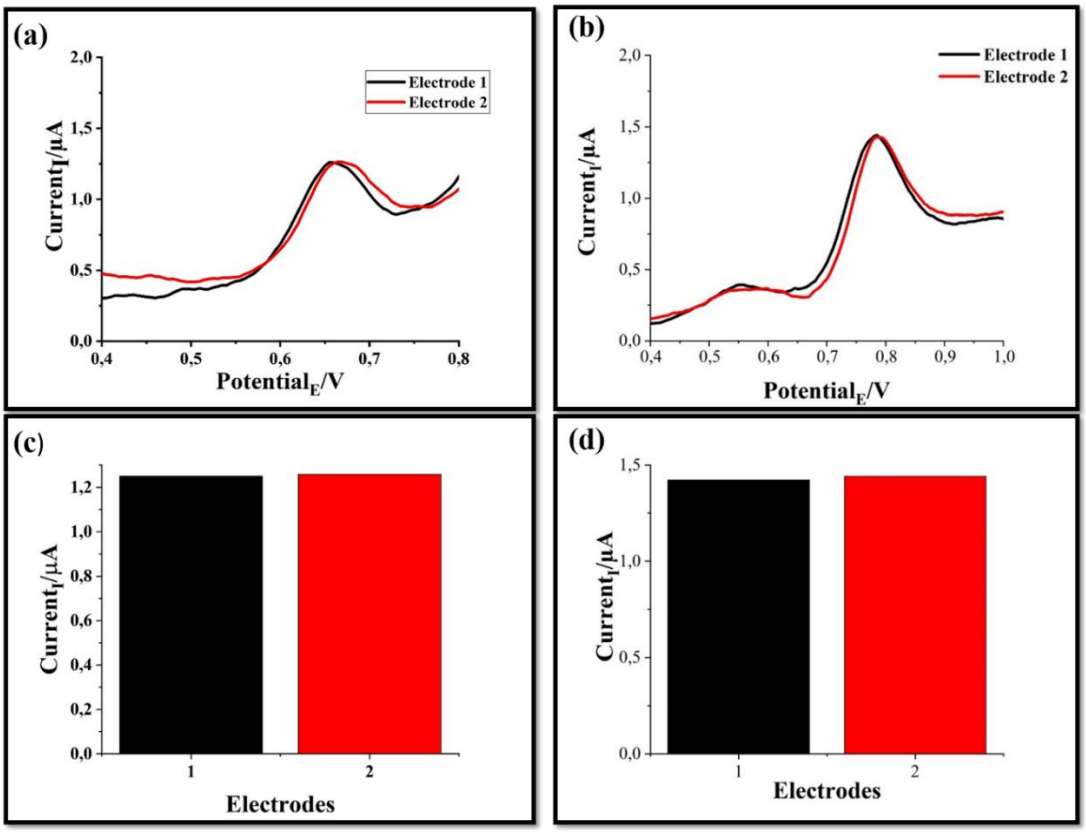

Figure 0.26: Differential pulse voltammograms of 0.04 mM RhB using Ni-DTBTA/GCE (a) 0.02 mM NiS/GCE @200 C (b) to demonstrate reproducibility.

Separelty two GCE were modified with NiS nanoparticles **Fig.3.26 (b)** under identical conditions and were then employed to determine 0.02 mM RhB. Obtained % standard deviation was found to be 0.697 % which indicate excellent reproducibility of the electrode modification. To check the repeatability the same NiS/GCE @200 °C was used in the determination of the RhB .In the two repeated experiments almost the same results were obtained with 0.50 %RSD for 0.02 mM RhB which indicates good repeatability for the proposed sensor similar (He et.,al 2019)reported on literature the use of nanoparticles for the detection of Rhodamine B.

CHAPTER 4

4. CONCLUSIONS AND RECOMMENDATIONS

4.1 Conclusion

Cadmium and nickel complexes were successfully synthesized and characterized by a combination of spectroscopic techniques. The benzothiazole complexes of cadmium and nickel were synthesized to be utilized as precursors for the preparation of cadmium and nickel sulphide nanoparticles. TGA, elemental analysis, melting point analysis FTIR and NMR spectroscopy were used for the characterization of the complexes. The elemental analysis showed the percentage of elements were within the acceptable limits. The ^{13}C NMR spectra for the prepared complexes showed a chemical shift on the CNS moiety of the complexes. The TGA curves show a single stable decomposition peak and the complexes decompose to form metal sulphide hence this suggest that the complexes can be used as potential precursors for synthesis of NiS and CdS nanoparticles.

The cadmium sulphide and nickel sulphide nanoparticles were successfully synthesized by thermal decomposition of 2.2-dithiobisbenzothiazole complexes in the presence of the capping agent. The temperatures of the reaction have a significant effect on the rate of the reaction that will affect the size and shape of the nanoparticles. This effect was confirmed by the optical properties of the synthesized nanoparticles prepared at different reaction temperatures. The spectra shows that absorption maximum and band edge shift to lower wavelength as the temperature of reaction was progressively increased. This trend is associated to the decrease in particles size of the prepared nanoparticles. TEM images further confirmed that the particles size of the prepared nanoparticles was progressively decreased as the temperature was increased. The time of the reaction is one of the most significant factors in the synthesis of the nanoparticles. The instigation of the time of the reaction yield results that depicted that with increase in time of the reaction, the band edge increases, but relatively at short wavelength to the bulk. Hence, the band edges of the nanoparticles were blue shifted significantly to the bulk. The results show that with an increase in the time of the reaction, the nanoparticles increases in their size due to Ostwald ripening. The XRD of the CdS nanoparticles produced at different reaction temperatures and different reaction times have the

same hexagonal phase. However different phases of nickel sulfide nanoparticles were observed when the temperature and time were varied.

EIS graphs were fitted using the randles circuit and they confirm that the NiS nanoparticles GCE greatly increase the electron transfer rate, probably due to the nanostructured surface property of the NiS nanoparticles. DPV showed that the current response of Rhb was higher for the optimum temperature NiS nanoparticles compared to all the materials used. There was an increase in the Rhb current response with an increase in pH and pH 7 was used as the optimum pH when Ni-complex was used as a modifier and pH 8 was used as optimum when NiS nanoparticles were used as a modifier. Effect of concentration showed that the NiS nanoparticles for the optimum temperature had a wide linear range and a low detection limit. The method has good accuracy, acceptable precision, and reproducibility. This method provides a novel electrochemical method for determination of RhB.

4.2 Recommendations

Based on the results and conclusions the following recommendations were made

Benzothiazole complexes should be purchased to prevent instability of the complexes and introduction of impurities during the preparation step, especially for early transition metals such as tungsten, molybdenum. Alternative synthesis chamber is required to enable the formation of the complexes without aerobic interferences that causes instability.

To investigate the effect of different capping molecule on the growth of these nanoparticles and what role do they play on the size and the shape of the nanoparticles. Particle shapes can also be dependent on the functionalities and length of the organic chains in organic molecules used as solvents and capping agents.

Investigate the effect temperature at above 300 °C using the same complexes of nickel and cadmium. Some interesting features appears to form at higher temperatures and therefore increasing the temperature can results in understanding the limiting factors in the control and growth of nanoparticles.

The developed electrochemical sensor must be tested in live samples to evaluate in practical applicability in the presence of different interfering agencies.

In order to reduce their charge transfer resistance and improve their electrochemical conductivity as well as electrochemical performance the nanoparticles must be incorporated with either carbonic material like graphene / carbon nanotubes or conducting polymers like PANI.

To develop a disposable electrochemical detection system, using pencil graphite electrode (PGEs) because they have a small diameter, inexpensive, disposable, high electrochemical reactivity, good mechanical rigidity compared to (GCE) that we used in this study.

5. REFERENCES

AGOSTIANO, A., CATALANO, M., CURRI, M. L., DELLA MONICA, M., MANNA, L., & VASANELLI, L. 2000. Synthesis and structural characterisation of CdS nanoparticles prepared in a four-components "water-in-oil" microemulsion. Micron, 31(3), 253–258. https://doi.org/10.1016/S0968-4328(99)00091-8

AL-KAHTANI, A. A. 2017. Photocatalytic Degradation of Rhodamine B Dye in Wastewater Using Gelatin/CuS/PVA Nanocomposites under Solar Light Irradiation. Journal of Biomaterials and Nanobiotechnology, 08(01), 66–82. https://doi.org/10.4236/jbnb.2017.81005

ALI, M. H. H., AL-AFIFY, A. D., & GOHER, M. E. 2018. Preparation and characterization of graphene – TiO2 nanocomposite for enhanced photodegradation of Rhodamine-B dye. Egyptian Journal of Aquatic Research, 44(4), 263–270. https://doi.org/10.1016/j.ejar.2018.11.009

ALRASHDI, A., FARGHALY, O., & BRANCH, A. (2020). Selective Preconcentration of Ultra Trace Copper (II) ion Using Square Wave Cathodic Adsorptive Stripping Voltammetry at Modified Carbon Past Electrode. January. https://doi.org/10.20964/2020.01.83

AMMAR, R. A., ALTURIQI, A. S., ALAGHAZ, A. M. A., & ZAYED, M. E. 2018. Synthesis , spectral characterization , quantum chemical calculations , in-vitro antimicrobial and DNA activity studies of 2- (2 0 -mercaptophenyl) benzothiazole complexes. 1168, 250–263. https://doi.org/10.1016/j.molstruc.2018.05.043

ANTOLINI, F., BURRESI, E., STROEA, L., MORANDI, V., ORTOLANI, L., ACCORSI, G., & BLOSI, M. 2012. Time and temperature dependence of CdS nanoparticles grown in a polystyrene matrix. Journal of Nanomaterials, 2012. https://doi.org/10.1155/2012/815696

BADDOUH, A., BESSEGATO, G. G., RGUITI, M. M., EL IBRAHIMI, B., BAZZI, L., HILALI, M., & ZANONI, M. V. B. 2018. Electrochemical decolorization of Rhodamine B dye: Influence of anode material, chloride concentration and current density. Journal of Environmental Chemical Engineering, 6(2), 2041–2047.

https://doi.org/10.1016/j.jece.2018.03.007

BESSEGATO, G. G., BRUGNERA, M. F., VALNICE, M., & ZANONI, B. 2019. ScienceDirect Electrochemistry Electroanalytical sensing of dyes and colorants. Current Opinion in Electrochemistry, 16, 134–142. https://doi.org/10.1016/j.coelec.2019.05.008

BHAT, S. A., RASHID, N., RATHER, M. A., BHAT, S. A., INGOLE, P. P., & BHAT, M. A. 2020. Highly efficient catalytic reductive degradation of Rhodamine-B over Palladium-reduced graphene oxide nanocomposite. Chemical Physics Letters, 754(May), 137724. https://doi.org/10.1016/j.cplett.2020.137724

BOBINIHI, F. F., FAYEMI, O. E., & ONWUDIWE, D. C. 2021. Synthesis, characterization, and cyclic voltammetry of nickel sulphide and nickel oxide nanoparticles obtained from Ni(II) dithiocarbamate. Materials Science in Semiconductor Processing, 121(May 2020), 105315. https://doi.org/10.1016/j.mssp.2020.105315

BOBINIHI, F. F., OSUNTOKUN, J., & ONWUDIWE, D. C. 2018. Syntheses and characterization of nickel(II) dithiocarbamate complexes containing NiS4 and NiS2PN moieties: Nickel sulphide nanoparticles from a single source precursor. Journal of Saudi Chemical Society, 22(4), 381–395. https://doi.org/10.1016/j.jscs.2017.10.001

CAI, Y., HUANG, W., & WU, K. 2020. Sensors and Actuators B : Chemical Morphology-controlled electrochemical sensing of erbium- benzenetricarboxylic acid frameworks for azo dyes and fl avonoids. Sensors & Actuators: B. Chemical, 304(September 2019), 127370. https://doi.org/10.1016/j.snb.2019.127370

CELINE ROSE, I. R., SATHISH, R., JEYA RAJENDRAN, A., & SAGAYARAJ, P. 2016. Effect of reaction time on the synthesis of cadmium selenide nanoparticles and the efficiency of solar cell. Journal of Materials and Environmental Science, 7(5), 1589–1596.

CHANG, Y., WANG, H., CHIU, C., CHENG, D., YEN, M., & CHIU, H. 2002. Low-Temperature Synthesis of Transition Metal Nanoparticles from Metal Complexes and Organopolysilane Oligomers. 26, 4334–4338.

CHAUHAN, R., GILL, A. A. S., NATE, Z., & KARPOORMATH, R. 2020. Highly selective

electrochemical detection of ciprofloxacin using reduced graphene oxide/poly(phenol red) modified glassy carbon electrode. Journal of Electroanalytical Chemistry, 871, 114254. https://doi.org/10.1016/j.jelechem.2020.114254

CHEN, Y., QIAN, J., WANG, N., XING, J., & LIU, L. 2020. In-situ synthesis of CNT/TiO2 heterojunction nanocomposite and its efficient photocatalytic degradation of Rhodamine B dye. Inorganic Chemistry Communications, 119, 108071. https://doi.org/10.1016/j.inoche.2020.108071

CRUZ TERRAZAS, E. C., LUQUE, P. A., CASTILLO, S. J., AMBROSIO LÁZARO, R. C., MOTA GONZÁLEZ, M. L., & CARRILLO-CASTILLO, A. 2015. A Simple Method For The Synthesis of CdS Nanoparticles Using A Novel Surfactant. Chalcogenide Letters, 12(4), 147–153.

DARAVATH, S., KUMAR, M. P., RAMBABU, A., VAMSIKRISHNA, N., GANJI, N., & SHIVARAJ. 2017. Design, synthesis, spectral characterization, DNA interaction and biological activity studies of copper(II), cobalt(II) and nickel(II) complexes of 6-amino benzothiazole derivatives. Journal of Molecular Structure, 1144(Ii), 147–158. https://doi.org/10.1016/j.molstruc.2017.05.022

DIN, M. I., & REHAN, R. 2017. Synthesis , Characterization , and Applications of Copper Nanoparticles. Analytical Letters, 50(1), 50–62. https://doi.org/10.1080/00032719.2016.1172081

DONDONI, A., & MERINO, P. 1996. Thiazoles. Comprehensive Heterocyclic Chemistry II: A Review of the Literature 1982-1995, 3, 373–474. https://doi.org/10.1016/B978-008096518-5.00064-2

GILL, A. A. S., SINGH, S., NATE, Z., CHAUHAN, R., THAPLIYAL, N. B., KARPOORMATH, R., MARU, S. M., & REDDY, T. M. 2020. A novel copper-based 3D porous nanocomposite for electrochemical detection and inactivation of pathogenic bacteria. Sensors and Actuators, B: Chemical, 321(March), 128449. https://doi.org/10.1016/j.snb.2020.128449

GOMAA, E. A., NEGM, A., & ABU-QARN, R. M. 2018. Cyclic voltammetry study of the electrochemical behavior of vanadyl sulfate in absence and presence of antibiotic. Measurement, 125(May), 645–650. https://doi.org/10.1016/j.measurement.2018.05.046

GOWTHAMAN, N. S. K., NGEE, H., BALAKUMAR, V., & SHANKAR, S. 2020. Ultrasonics - Sonochemistry Ultrasonic synthesis of CeO 2 @ organic dye nanohybrid : Environmentally benign rabid electrochemical sensing platform for carcinogenic pollutant in water samples. Ultrasonics - Sonochemistry, 61(August 2019), 104828. https://doi.org/10.1016/j.ultsonch.2019.104828

HABILA, M. A., YILMAZ, E., ALOTHMAN, Z. A., & SOYLAK, M. (2016). Combination of dispersive liquid-liquid microextraction and multivariate optimization for separation-enrichment of traces lead by flame atomic absorption spectrometry. Journal of Industrial and Engineering Chemistry, 37, 306–311. https://doi.org/10.1016/j.jiec.2016.03.037

HE, Q., LIU, J., LIU, X., XIA, Y., LI, G., & DENG, P. (N.D.). Novel Electrochemical Sensors Based on Cuprous Oxide-Electrochemically Reduced Graphene Oxide Nanocomposites Modified Electrode toward Sensitive. https://doi.org/10.3390/molecules23092130

HE, Q., LIU, J., TIAN, Y., WU, Y., MAGESA, F., DENG, P., & LI, G. 2019. Facile preparation of cu2o nanoparticles and reduced graphene oxide nanocomposite for electrochemical sensing of rhodamine b. Nanomaterials, 9(7). https://doi.org/10.3390/nano9070958

HU, S., XU, D., ZHOU, J., DU, S., ZHAO, K., LI, H., CHEN, R., & ZHOU, D. 2021. A simple coordination complex-derived NiS nanocatalyst for reduction of 4-nitrophenol and methyl orange. Inorganic Chemistry Communications, 125(November 2020), 108428. https://doi.org/10.1016/j.inoche.2020.108428

JEJENIJA, O. 2016. Synthesis and char acterization of group 12 dithiolate complexes as single source precursor s for the preparation of hexadecylamine capped metal sulfide nanoparti cles and polymer nanocomposites Synthesis and char acterization of group 12 dithiolate compl. January.

KAWDE, A., BAIG, N., & SAJID, M. 2016. RSC Advances Graphite pencil electrodes as

electrochemical sensors for environmental analysis : a review of features , developments , and applications. RSC Advances, 6, 91325–91340. https://doi.org/10.1039/C6RA17466C

KHAN, S., WONG, A., VALNICE, M., ZANONI, B., DEL, M., & TABOADA, P. 2019. Materials Science & Engineering C Electrochemical sensors based on biomimetic magnetic molecularly imprinted polymer for selective quanti fi cation of methyl green in environmental samples. Materials Science & Engineering C, 103(February), 109825. https://doi.org/10.1016/j.msec.2019.109825

KLEIJN, S. E. F., LAI, S. C. S., KOPER, M. T. M., & UNWIN, P. R. 2014. Electrochemistry of Nanoparticles Angewandte. 3558–3586. https://doi.org/10.1002/anie.201306828

KRISTL, M., DOJER, B., GYERGYEK, S., & KRISTL, J. 2017. Synthesis of nickel and cobalt sulfide nanoparticles using a low cost sonochemical method. Heliyon, 3(3), 1–19. https://doi.org/10.1016/j.heliyon.2017.e00273

KUCUR, E., RIEGLER, J., URBAN, G. A., & NANN, T. 2003. Determination of quantum confinement in CdSe nanocrystals by cyclic voltammetry. Journal of Chemical Physics, 119(4), 2333–2337. https://doi.org/10.1063/1.1582834

KUMAR, S., SHARMA, J. K., SHARMA, S. K., DHUPAR, A., SHARMA, V., & GAUR, A. 2020. Structural, electrical and magnetic properties of glucose-capped CdS nanoparticles. International Journal of Materials Research, 111(10), 799–806. https://doi.org/10.3139/146.111943

KURIAN, P. A., VIJAYAN, C., SATHIYAMOORTHY, K., SUCHAND SANDEEP, C. S., & PHILIP, R. 2007. Excitonic transitions and off-resonant optical limiting in CdS quantum dots stabilized in a synthetic glue matrix. Nanoscale Research Letters, 2(11), 561–568. https://doi.org/10.1007/s11671-007-9099-8

KURZAJEWSKA, M., KWIATEK, D., KUBICKI, M., BRZEZINSKI, B., & HNATEJKO, Z. 2018. New complexes of 2- (4-pyridyl) -1 , 3-benzothiazole with metal ions ; synthesis , structural and spectral studies. 148, 1–8. https://doi.org/10.1016/j.poly.2018.03.024

KUZNETSOVA, Y. V., LETOFSKY-PAPST, I., SOCHOR, B., SCHUMMER, B., SERGEEV,

A. A., HOFER, F., & REMPEL, A. A. 2019. Greatly enhanced luminescence efficiency of CdS nanoparticles in aqueous solution. Colloids and Surfaces A: Physicochemical and Engineering Aspects, 581(August), 123814. https://doi.org/10.1016/j.colsurfa.2019.123814

LET, A. L., Ã, D. E. M., RIX, C. J., & MURUGARAJ, P. 2007. Thio sol – gel synthesis of titanium disulfide thin films and nanoparticles using titanium (IV) alkoxide precursors. 68, 1428–1435. https://doi.org/10.1016/j.jpcs.2007.03.001

LI, M., GOU, H., AL-OGAIDI, I., & WU, N. 2013. Nanostructured Sensors for Detection of Heavy Metals: A Review.

MANDAL, T., STAVILA, V., RUSAKOVA, I., GHOSH, S., & WHITMIRE, K. H. 2009. Molecular precursors for cds nanoparticles: synthesis and characterization of carboxylate - Thiourea or - Tcadmium complexes and their decomposition. Chemistry of Materials, 21(23), 5617–5626. https://doi.org/10.1021/cm902230u

MANICKATHAI, K., VISWANATHAN, S. K., & ALAGAR, M. 2008. Synthesis and characterization of CdO and CdS nanoparticles. 46(August), 561–564.

MARCONATO, J. C., BULHÕES, L. O., & TEMPERIN, M. L. 1997. A spectroelectrochemical study of the inhibition of the electrode process on copper by 2-mercaptobenzothiazole in ethanolic solutions. Electrochimica Acta, 43(7), 771–780. https://doi.org/10.1016/S0013-4686(97)00204-1

MARINESCU, C., BEN ALI, M., HAMDI, A., CHERIFI, Y., BARRAS, A., COFFINIER, Y., SOMACESCU, S., RADITOIU, V., SZUNERITS, S., & BOUKHERROUB, R. 2018. Cobalt phthalocyanine-supported reduced graphene oxide: A highly efficient catalyst for heterogeneous activation of peroxymonosulfate for rhodamine B and pentachlorophenol degradation. Chemical Engineering Journal, 336, 465–475. https://doi.org/10.1016/j.cej.2017.12.009

MENSAH, M. B., AWUDZA, J. A. M., REVAPRASADU, N., & O'BRIEN, P. 2021. Synthesis of CdS and PbS nanoparticles by the thermal decomposition of ethyl xanthate complexes in castor oil using the heat-up technique. Materials Science in Semiconductor Processing,

122(October 2020), 105493. https://doi.org/10.1016/j.mssp.2020.105493

MESHRAM, S. D., RUPNARAYAN, R. V, & JAGTAP, S. V. 2015. Synthesis and Characterization of Lead Oxide Nanoparticles. 4, 83–88.

MOLOTO, N., REVAPRASADU, N., MUSETHA, P. L., & MOLOTO, M. J. 2009. The effect of precursor concentration, temperature and capping group on the morphology of CdS nanoparticles. Journal of Nanoscience and Nanotechnology, 9(8), 4760–4766. https://doi.org/10.1166/jnn.2009.219

NAJA, H., & BAHARI, A. 2016. Optical and cyclic voltammetry behavior studies on nanocomposite fi lm of copolymer and WO 3 grown by electropolymerization. 217, 19–28. https://doi.org/10.1016/j.synthmet.2016.03.008

NANDHINI, S., & MURALIDHARAN, G. 2018. Surfactant free nickel sulphide nanoparticles for high capacitance supercapacitors. AIP Conference Proceedings, 1942, 1–5. https://doi.org/10.1063/1.5029191

NATE, Z., GILL, A. A. S., SHINDE, S., CHAUHAN, R., INAMDAR, S. N., & KARPOORMATH, R. 2021. A simple in-situ flame synthesis of nanocomposite (MWCNTs-Fe2O3) for electrochemical sensing of proguanil in pharmaceutical formulation. Diamond and Related Materials, 111(November 2020), 108178. https://doi.org/10.1016/j.diamond.2020.108178

NQOMBOLO, A., & AJIBADE, P. A. 2016. Synthesis and Spectral Studies of Ni(II) Dithiocarbamate Complexes and Their Use as Precursors for Nickel Sulphides Nanocrystals. Journal of Chemistry, 2016. https://doi.org/10.1155/2016/1293790

NYAMEN, L. D., REVAPRASADU, N., PULLABHOTLA, R. V. S. R., NEJO, A. A., NDIFON, P. T., MALIK, M. A., & O'BRIEN, P. 2013. Synthesis of multi-podal CdS nanostructures using heterocyclic dithiocarbamato complexes as precursors. Polyhedron, 56, 62–70. https://doi.org/10.1016/j.poly.2013.03.027

ONWUDIWE, D. C., HRUBARU, M., & EBENSO, E. E. 2015. Synthesis, Structural and Optical Properties of TOPO and HDA Capped Cadmium Sulphide Nanocrystals, and the Effect of

Capping Ligand Concentration. Journal of Nanomaterials, 2015. https://doi.org/10.1155/2015/143632

PATHAN, A. A., DESAI, K. R., & BHASIN, C. P. B. P. 2018. Improved Photocatalytic Properties of NiS Nanocomposites Prepared by Displacement Method for Removal of Rose Bengal Dye. Current Nanomaterials, 2(3), 169–176. https://doi.org/10.2174/2405461503666180420115141

PAWAR, A. S., MASIKANE, S. C., MLOWE, S., GARJE, S. S., & REVAPRASADU, N. 2016. Preparation of CdS Nanoparticles from Thiosemicarbazone Complexes: Morphological Influence of Chlorido and Iodido Ligands. European Journal of Inorganic Chemistry, 2016(3), 366–372. https://doi.org/10.1002/ejic.201501125

PAWAR, M. J., INGLE, A. D., & TAYAWADE, R. K. 2019. Effect of Synthesis Parameters on Photoactivity of CdS Nanoparticles. Chemical Science Transactions, 8(2), 219–227. https://doi.org/10.7598/cst2019.1549

QI, L., CÖLFEN, H., & ANTONIETTI, M. 2001. Synthesis and Characterization of CdS Nanoparticles Stabilized by Double-Hydrophilic Block Copolymers. Nano Letters, 1(2), 61–65. https://doi.org/10.1021/nl0055052

REYES, P. Y., PUENTE-URBINA, B., & AVILA-ORTA, C. A. 2014. Synthesis of Copper Nanoparticles by Thermal Decomposition and Their Antimicrobial Properties Synthesis of Copper Nanoparticles by Thermal Decomposition and Their Antimicrobial Properties. January 2013. https://doi.org/10.1155/2013/980545

RIYAZ, S., PARVEEN, A., & AZAM, A. 2016. Microstructural and optical properties of CuS nanoparticles prepared by sol — gel route ☪. Perspectives in Science, 8, 632–635. https://doi.org/10.1016/j.pisc.2016.06.041

ROFFEY, A., HOLLINGSWORTH, N., ISLAM, H. U., MERCY, M., SANKAR, G., CATLOW, C. R. A., HOGARTH, G., & DE LEEUW, N. H. 2016. Phase control during the synthesis of nickel sulfide nanoparticles from dithiocarbamate precursors. Nanoscale, 8(21), 11067–11075. https://doi.org/10.1039/c6nr00053c

ROY, A., DIGE, S., UMARJI, G. G., SHINDE, M. D., RANE, S. B., MULIK, U. P., AMALNERKAR, D. P., & CHAUHAN, R. 2015. Solvothermal Syntheses of Cadmium Sulfide Nanoparticles with Varying Concentration of Ammonia and Reaction Time and Their Effect on Optical Properties. Materials Focus, 4(2), 142–149. https://doi.org/10.1166/mat.2015.1230

RUBINO, S., BUSÀ, R., ATTANZIO, A., ALDUINA, R., DI STEFANO, V., GIRASOLO, M. A., ORECCHIO, S., & TESORIERE, L. 2017. Synthesis, properties, antitumor and antibacterial activity of new Pt(II) and Pd(II) complexes with 2,2′-dithiobis(benzothiazole) ligand. Bioorganic and Medicinal Chemistry, 25(8), 2378–2386. https://doi.org/10.1016/j.bmc.2017.02.067

RUBINO, S., SALADINO, M. L., BUSÀ, R., CHILLURA MARTINO, D. F., GIRASOLO, M. A., CAPONETTI, E., TESORIERE, L., & ATTANZIO, A. 2018. Loading and release of the complex [Pt(DTBTA)(DMSO)Cl]Cl·CHCl3 with the 2,2′-dithiobis(benzothiazole) ligand into mesoporous silica and studies of antiproliferative activity on MCF-7 cells. Polyhedron, 153, 234–239. https://doi.org/10.1016/j.poly.2018.07.006

SALAVATI-NIASARI, M., BANAIEAN-MONFARED, G., EMADI, H., & ENHESSARI, M. 2013. Synthesis and characterization of nickel sulfide nanoparticles via cyclic microwave radiation. Comptes Rendus Chimie, 16(10), 929–936. https://doi.org/10.1016/j.crci.2013.01.011

SALAVATI-NIASARI, M., & SOBHANI, A. 2012. Single-source molecular precursor for synthesis of cds nanoparticles and nanoflowers. High Temperature Materials and Processes, 31(2), 157–162. https://doi.org/10.1515/htmp-2011-0157

SANTRA, A., BRANDAO, P., MONDAL, G., BERA, P., JANA, A., BHATTACHARYYA, I., PRAMANIK, C., & BERA, P. 2020. Monomeric and dimeric cadmium(II) complexes of S-alkyl/aryl dithiocarbazate as single-source precursors for cadmium sulfide nanoparticles: An experimental, theoretical interpretation in the stability of precursor and visible light dye degradation study. Inorganica Chimica Acta, 501(August 2019), 119315. https://doi.org/10.1016/j.ica.2019.119315

SATHIYARAJ, E., THIRUMARAN, S., CIATTINI, S., & SELVANAYAGAM, S. 2019. Synthesis and characterization of Ni(II) complexes with functionalized dithiocarbamates: New single source precursors for nickel sulfide and nickel-iron sulfide nanoparticles. Inorganica Chimica Acta, 498(April). https://doi.org/10.1016/j.ica.2019.119162

SATHIYARAJ, ETHIRAJ, PADMAVATHY, K., KUMAR, C. U., KRISHNAN, K. G., & RAMALINGAN, C. 2017. Synthesis and spectral studies on Cd(II) dithiocarbamate complexes and their use as precursors for CdS nanoparticles. Journal of Molecular Structure, 1147(Ii), 103–113. https://doi.org/10.1016/j.molstruc.2017.06.080

SENGAN, M., & VEERAPPAN, A. 2019. N-myristoyltaurine capped copper nanoparticles for selective colorimetric detection of Hg 2+ in wastewater and as effective chemocatalyst for organic dye degradation. Microchemical Journal, 148(February), 1–9. https://doi.org/10.1016/j.microc.2019.04.049

SHAH, A. 2020. A Novel Electrochemical Nanosensor for the Simultaneous Sensing of Two Toxic Food Dyes. https://doi.org/10.1021/acsomega.0c00354

SHETTI, N. P., MALODE, S. J., MALLADI, R. S., NARGUND, S. L., SHUKLA, S. S., & AMINABHAVI, T. M. 2019. Electrochemical detection and degradation of textile dye Congo red at graphene oxide modified electrode Structure of Congo Red Dye a Potential / V. Microchemical Journal, 146(January), 387–392. https://doi.org/10.1016/j.microc.2019.01.033

SHIRMOHAMMADZADEH, L. K. L. (2017). Synthesis of Co (II) and Cr (III) salicylidenic Schiff base complexes derived from thiourea as precursors for nano-sized Co 3 O 4 and Cr 2 O 3 and their catalytic , antibacterial properties. Journal of Nanostructure in Chemistry, 7(2), 179–190. https://doi.org/10.1007/s40097-017-0221-x

SHOMBE, G. B., KHAN, M. D., ZEQUINE, C., ZHAO, C., GUPTA, R. K., & REVAPRASADU, N. 2020. Direct solvent free synthesis of bare α-NiS, β-NiS and α-β-NiS composite as excellent electrocatalysts: Effect of self-capping on supercapacitance and overall water

splitting activity. *Scientific Reports*, *10*(1), 1–14. https://doi.org/10.1038/s41598-020-59714-9

SHOMBE, G. B., MUBOFU, E. B., MLOWE, S., & REVAPRASADU, N. 2016. Synthesis and characterization of castor oil and ricinoleic acid capped CdS nanoparticles using single source precursors. Materials Science in Semiconductor Processing, 43, 230–237. https://doi.org/10.1016/j.mssp.2015.11.011

SITHOLE, R. K., MACHOGO, L. F. E., AIRO, M. A., GQOBA, S. S., MOLOTO, M. J., SHUMBULA, P., VAN WYK, J., & MOLOTO, N. 2018. Synthesis and characterization of Cu3N nanoparticles using pyrrole-2-carbaldpropyliminato Cu(II) complex and Cu(NO3)2 as single-source precursors: The search for an ideal precursor. New Journal of Chemistry, 42(4), 3042–3049. https://doi.org/10.1039/c7nj05181f

STENGER-SMITH, J., CHAKRABORTY, I., & MASCHARAK, P. K. 2018. Cationic Au (I) complexes with aryl-benzothiazoles and their antibacterial activity. Journal of Inorganic Biochemistry, 185(May), 80–85. https://doi.org/10.1016/j.jinorgbio.2018.05.003

SURESH, S. 2013. Semiconductor Nanomaterials, Methods and Applications: A Review. Nanoscience and Nanotechnology, 3(3), 62–74. https://doi.org/10.5923/j.nn.20130303.06

TARIQ, M., MUHAMMAD, M., KHAN, J., RAZIQ, A., UDDIN, M. K., NIAZ, A., AHMED, S. S., & RAHIM, A. 2020. Removal of Rhodamine B dye from aqueous solutions using photo-Fenton processes and novel Ni-Cu@MWCNTs photocatalyst. Journal of Molecular Liquids, 312, 113399. https://doi.org/10.1016/j.molliq.2020.113399

THANGWANE, C. S., XABA, T., & MOLOTO, M. J. 2017. the Formation of the Mixed Morphology of Nickel Sulfide Nanoparticles Derived From Substituted Benzimidazole Dithiocarbamate Nickel (Ii) Complexes. Chalcogenide Letters, 14(9), 407–417.

TRAN, H. V, HUYNH, C. D., TRAN, H. V, & PIRO, B. 2018. Cyclic voltammetry , square wave voltammetry , electrochemical impedance spectroscopy and colorimetric method for hydrogen peroxide detection based on chitosan / silver nanocomposite. Arabian Journal of

Chemistry, 11(4), 453–459. https://doi.org/10.1016/j.arabjc.2016.08.007

UCHIDA, Y., KÄTELHÖN, E., & COMPTON, R. G. 2018. Cyclic voltammetry with non-triangular waveforms : Electrochemically irreversible and quasi-reversible systems. Journal of Electroanalytical Chemistry, 810(December 2017), 135–144. https://doi.org/10.1016/j.jelechem.2017.12.053

UNSAL, Y. E., SOYLAK, M., & TUZEN, M. 2014. Spectrophotometric detection of rhodamine B after separation-enrichment by using multi-walled carbon nanotubes. Journal of AOAC International, 97(5), 1459–1462. https://doi.org/10.5740/jaoacint.12-458

WASLY, H. S., EL-SADEK, M. S. A., & HENINI, M. 2018. Influence of reaction time and synthesis temperature on the physical properties of ZnO nanoparticles synthesized by the hydrothermal method. Applied Physics A: Materials Science and Processing, 124(1). https://doi.org/10.1007/s00339-017-1482-4

XABA, T., MOLOTO, M. J., AL-SHAKBAN, M., MALIK, M. A., BRIEN, P. O., & MOLOTO, N. 2017. Materials Science in Semiconductor Processing The e ff ect of temperature on the growth of Ag 2 O nanoparticles and thin fi lms from bis (2-hydroxy-1-naphthaldehydato) silver (I) complex by the thermal decomposition of spin – coated fi lms. 71(April), 109–115. https://doi.org/10.1016/j.mssp.2017.07.015

YANG, X., YANG, Y., WANG, B., WANG, T., WANG, Y., & MENG, D. 2019. Synthesis and photocatalytic property of cubic phase CdS. Solid State Sciences, 92(March), 31–35. https://doi.org/10.1016/j.solidstatesciences.2019.04.004

YOUSIF, E., MAJEED, A., AL-SAMMARRAE, K., SALIH, N., SALIMON, J., & ABDULLAH, B. (2017). Metal complexes of Schiff base : Preparation , characterization and antibacterial activity. Arabian Journal of Chemistry, 10, S1639–S1644. https://doi.org/10.1016/j.arabjc.2013.06.006

ZHAO, X., & ZHU, Y. 2006. Synergetic degradation of rhodamine B at a porous ZnWO4 film electrode by combined electro-oxidation and photocatalysis. Environmental Science and Technology, 40(10), 3367–3372. https://doi.org/10.1021/es052029e